AIMS Mathematics, 11(4): 9942–9988.
DOI: 10.3934/math.2026411
Received: 26 January 2026
Revised: 24 March 2026
Accepted: 07 April 2026
Published: 13 April 2026

http://www.aimspress.com/journal/Math

Research article

A new discrete Pham model for nonmonotone aging and overdispersion: theory, inference, optimization, and three scientific applications

Ahmed Elshahhat[1,*], **Osama E. Abo-Kasem**[2] **and Heba S. Mohammed**[3]

[1] Faculty of Technology and Development, Zagazig University, Zagazig 44519, Egypt

[2] Department of Statistics, Faculty of Commerce, Zagazig University, Zagazig 44519, Egypt

[3] Department of Mathematical Sciences, College of Science, Princess Nourah bint Abdulrahman University, P.O. Box 84428, Riyadh 11671, Saudi Arabia

* **Correspondence:** Email: aelshahhat@ftd.zu.edu.eg.

Abstract: Discrete lifetime data arising in engineering reliability, biomedical studies, and risk-based applications often display nonmonotone aging behavior, heavy tails, and substantial overdispersion, which challenge the adequacy of classical discrete models. To overcome these limitations, the paper proposes a new discrete Pham (DPham) distribution obtained through survival-function discretization of the continuous Pham model. This construction yields a parsimonious yet highly flexible two-parameter discrete lifetime family that substantially extends the modeling capacity of existing discrete distributions. A central contribution of the DPham model is its ability to accommodate a wide range of hazard rate shapes, including decreasing, increasing, constant, and bathtub forms, within a single, unified framework. This flexibility allows the model to capture complex aging mechanisms such as early-failure dominance, intermediate-life stabilization, and long-tailed persistence while retaining analytical tractability. The probability mass function supports both monotone and unimodal configurations, enhancing its descriptive power in discrete settings. The paper develops comprehensive distributional properties of the DPham distribution, including quantile representation, dispersion characteristics, skewness, kurtosis, and order statistics, demonstrating a level of adaptability that exceeds that of commonly used discrete lifetime models. Inferential procedures are systematically explored under both likelihood-based and Bayesian frameworks, with explicit consideration of Type-II censored data. Bayesian estimation, implemented using Markov iterative algorithms, is shown to provide improved estimation accuracy and more reliable interval estimates, particularly in small-sample and heavily censored scenarios. The practical utility of the DPham distribution is illustrated through applications to real datasets from clinical survival analysis, industrial reliability systems, and overdispersed risk data. Across all cases, the proposed model consistently outperforms nine established discrete competitors, including discrete Weibull-type and gamma-based models, in terms of goodness of fit, inferential stability, and robustness to extreme observations. Supported by extensive simulation

evidence, these results establish the DPham distribution as a versatile and domain-agnostic tool for discrete lifetime modeling, offering a compelling alternative for reliability theory, biostatistics, and applied risk analysis.

Keywords: Pham; V-tub shaped; survival; hazard; Bayesian; likelihood; normality and log-normality; moments; order statistics; optimization; Markov chain; Newton-Raphson; censoring; data applicability
Mathematics Subject Classification: 60E05, 62E10, 62N01, 62N05, 62P10

1. Introduction

Pham (or log-log) distribution, originally proposed by Pham [1], is a lifespan constructed to outperform classical models (exponential, gamma, or Weibull) by introducing additional shape parameters that allow greater control over the failure rate (FR) behavior and improved modeling of complex aging mechanisms in real systems. In its general philosophy, it is obtained by transforming a baseline distribution (often of an exponential type) through power or nonlinear operators, leading to richer structural properties. Conceptually, it belongs to the class of generalized exponential-type distributions designed to overcome the rigidity of adverse FR modes. A V-tub (bathtub) shape is one of the most significant benefits of the Pham model. This FR style is a representative pattern in survival analysis in which the FR initially decreases, subsequently remains approximately constant for a certain duration, and ultimately increases. Such behavior is frequently encountered in empirical data, particularly in engineering applications and reliability studies. See, for more details, Srivastava and Kumar [2]. Although classical lifetime distributions such as the gamma, Weibull, and lognormal models have been extensively employed in reliability and survival analysis, they often exhibit inherent limitations in capturing complex aging behaviors, particularly nonmonotone FR structures such as the V-tub shape. These models typically require additional parameters or composite constructions to accommodate such features, which may compromise interpretability and increase model complexity. In contrast, the Pham distribution provides a unified and flexible framework capable of modeling decreasing, constant, increasing, and V-tub shaped FRs within a parsimonious parameterization. This intrinsic flexibility makes it particularly appealing for representing real-world systems characterized by early-life failures, periods of stability, and eventual wear-out phenomena. From a discretization perspective, the choice of the baseline continuous distribution plays a crucial role in determining the structural properties of the resulting discrete model. By adopting the Pham distribution, the proposed discrete analog inherits several desirable features, including enhanced control over skewness and tail behavior, the ability to accommodate overdispersion, and the preservation of complex FR dynamics.

Discrete lifetime and count data naturally arise in various applied fields, including reliability engineering (e.g., Yang et al. [3]), actuarial science (e.g., La Rocca [4]), epidemiology (e.g., Singh et al. [5]), and quality control (e.g., Yang et al. [6]). Discretization refers to the process of transforming continuous probability distributions into a finite set of representative mass points. This approach is particularly useful when evaluating models that are computationally intensive or when complete distributional information is unavailable. Typically, the procedure involves two steps (see Keefer and Bodily [7]): first, selecting discretization points, often based on percentiles of the underlying

continuous distribution, and second, assigning probability masses to these points accordingly. Discrete distributions are especially valuable for simulating lifespan or count data in such contexts. Their utility has led to widespread application of discretization techniques. By partitioning a probability distribution into intervals based on values or cumulative probabilities, the distribution can be rendered discrete. Percentiles are commonly allocated to the mean or median of each interval, and the corresponding probability mass is assigned according to the interval's size (see Lai [8]). Common discrete analogs of continuous distributions include the geometric and negative binomial distributions, often used as substitutes for the gamma and exponential distributions. However, these discrete counterparts do not always capture empirical patterns accurately. Consequently, a number of continuous lifetime distributions have recently been discretized to develop more flexible discrete models capable of accurately representing real-world phenomena, such as accident counts, ecological species frequencies, insurance claims, and longevity data, all of which exhibit discrete counts.

Various discretization techniques have been proposed to convert continuous models into discrete equivalents, and these approaches have been extensively investigated; see, for instance, Jayakumar and Sankaran [9], Afify et al. [10], and Taconeli and Rodrigues de Lara [11], among others. A particularly prominent approach for constructing discrete distributions involves using the survival function (SF) framework. Notable contributions in this area include discrete analogs of the normal and Rayleigh distributions, as developed by Roy [12, 13]. Further extensions have been proposed for a variety of distributions: Bebbington et al. [14] for the discrete additive Weibull, Haj Ahmad and Elshahhat [15] for the discrete Hjorth, Eldeeb et al. [16] for the discrete XLindley, and Elshahhat et al. [17, 18] for the discrete Gompertz-Makeham and discrete Maxwell-Boltzmann distributions, respectively. These studies collectively illustrate the versatility and applicability of discrete transformations across diverse distributional frameworks.

Although several discrete distributions have been proposed in the literature, many classical models remain limited in their ability to capture complex failure behaviors such as overdispersion, skewness, and nonmonotone hazard rate structures. Motivated by these challenges and by the flexibility of the continuous Pham distribution in reliability modeling, the next section introduces a new discrete Pham (DPham) distribution as a viable and analytically tractable alternative for modeling discrete lifetime phenomena. The proposed model inherits the structural flexibility of its continuous counterpart while offering richer hazard rate behavior and improved fit performance compared to existing discrete distributions. Moreover, its parameters retain clear interpretability, facilitating practical implementation and inferential analysis. These features make the DPham distribution a competitive and robust tool for modeling discrete reliability data. Although classical discrete models (e.g., geometric, negative binomial, etc.) are computationally convenient, they often fail to capture complex data features such as nonmonotone hazard structures, overdispersion, heavy tails, and strong skewness. On the other hand, continuous lifetime models, particularly the Pham distribution, have demonstrated remarkable flexibility in modeling realistic aging mechanisms through their ability to exhibit decreasing, increasing, constant, and V-tub shaped failure rates.

However, the direct applicability of such continuous models is limited when data are inherently discrete or recorded in integer-valued form. This gap motivates the development of a discrete analog that preserves the essential flexibility of the continuous Pham model while remaining analytically tractable and practically relevant for discrete data. Across the three real-data applications drawn from clinical trials, industrial engineering, and count-based risk analysis, the DPham model consistently

outperformed several competing discrete models, such as discrete gamma, discrete Nadarajah-Haghighi, and discrete modified Weibull, among others, in terms of goodness-of-fit and inferential stability. Its ability to simultaneously accommodate nonmonotone hazard behavior, overdispersion, and heavy-tailed counts led to markedly improved empirical performance, particularly in datasets exhibiting early failures, extreme observations, or incomplete sampling. These results collectively demonstrate that the DPham distribution provides a more flexible and robust modeling framework than existing discrete alternatives when confronted with complex and sector-diverse real-world data. The present study addresses this need by proposing a new DPham distribution and demonstrating its inferential and modeling advantages through theoretical development, simulation assessment, and applications to three real-world problems exhibiting diverse and challenging data characteristics. The primary contributions of this study can be categorized into seven key areas, as outlined below:

- A novel discrete lifetime model is proposed via a survival discretization of the continuous Pham distribution, yielding a flexible and interpretable probability mass function suitable for integer-valued observations.
- The DPham hazard rate rigorously preserves behaviors of the continuous Pham, including increasing, constant, and V-tub (bathtub) patterns, thereby extending complex aging mechanisms to the discrete framework. Its mass function can be decreasing, increasing, or unimodal depending on parameter configurations, providing substantial adaptability for modeling diverse count data.
- Main characteristics, including the hazard rate, closed-form quantile function, moments, dispersion index, coefficient of variation, skewness, and kurtosis, are developed, offering comprehensive insight into the distribution's behavior. Explicit expressions for order statistics, particularly minimum and maximum values, are also derived and analyzed.
- Maximum likelihood estimation (MLE) is formulated for Type-II censored (CT2) samples, and the existence and uniqueness of the resulting estimators are formally proven, ensuring inferential reliability in practical life-testing scenarios. A full Bayesian estimation framework is developed using gamma priors and Metropolis-Hastings algorithms, enabling efficient posterior inference when closed-form solutions are unavailable.
- Two bounds of asymptotic confidence interval (ACI), Bayesian credible interval (BCI), and highest posterior density (HPD) are constructed and compared, highlighting the superior performance of Bayesian intervals in terms of coverage accuracy and interval length.
- A comprehensive simulation study investigates the behavior of point and interval estimators across varying sample sizes, censoring levels, and prior specifications, demonstrating the robustness and efficiency of the proposed methods.
- The utility and practical relevance of the DPham model are demonstrated using three real datasets representing discrete lifetime data with nonmonotone aging behavior. In all cases, the DPham distribution provides improved fit, greater flexibility, and more reliable inference compared to commonly used discrete models.

The paper is structured as follows: Sections 2 and 3 present the DPham and its characteristics, respectively; Sections 4 and 5 derive the point and interval inferences, respectively; Section 6 lists the simulation experiments; Section 7 applies three real-world scenarios; and Section 8 ends the study with recommendations, remarks, and potential research.

2. New DPham distribution

Recall that the Pham model provides a flexible framework for modeling such systems due to its V-tub shaped FR, characterized by an initial decreasing phase, a plateau, and a final increasing phase. This structure aligns naturally with the three life stages of components, enabling preventive maintenance during early-life, condition-based monitoring in the useful-life, and planned replacements in the wear-out phase; see Fayomi et al. [19]. This part introduces the DPham distribution, which successfully mirrors the hazard and density flexibilities of the continuous Pham distribution, including V-tub shaped, increasing, and constant hazard rates in addition to decreasing, unimodal, and approximately symmetric. The shapes are consistent with the original distribution, with slight stepwise artifacts due to discreteness. Building on this development, the present study introduces a discrete analog of the DPham distribution to maintain the flexibility of its continuous counterpart while specifically addressing integer-valued observations. This advancement broadens its applicability to reliability analysis, count processes, and practical contexts where data are inherently discrete.

Suppose Y is a nonnegative, random variable that follows the Pham($\boldsymbol{\theta}$) distribution, where $\boldsymbol{\theta} = (\alpha, \mu)^\top$ with $\alpha > 0$ (shape) and $\mu > 1$ (scale). For the continuous random variable Pham Y, we briefly define the probability density function (PMF, $g(\cdot)$) and the cumulative distribution function (CDF, $G(\cdot)$) for $y > 0$ as follows:

$$g(y;\boldsymbol{\theta}) = \alpha \log(\mu)\, \mu^{y^\alpha} y^{\alpha-1} e^{1-\mu^{y^\alpha}},\ y > 0, \tag{2.1}$$

and

$$G(y;\boldsymbol{\theta}) = 1 - e^{1-\mu^{y^\alpha}},\ y > 0, \tag{2.2}$$

respectively; for additional details, see Alqasem et al. [20] and Djeumeni et al. [21].

Then, its SF (say, S), for $y > 0$, is

$$\mathsf{S}(y;\boldsymbol{\theta}) = e^{1-\mu^{y^\alpha}}. \tag{2.3}$$

Now, by employing an SF-based discretization approach, the resulting model retains essential structural features such as flexibility in skewness and tail behavior while offering a better fit than traditional discrete distributions such as the Poisson, binomial, geometric, or negative binomial. A variety of techniques have been proposed for discretizing continuous distribution models, with the SF-based method emerging as particularly influential. This framework forms the foundation for deriving the discrete analog of the model. Building on this approach, we introduce a novel DPham($\boldsymbol{\theta}$) model and explore its key characteristics, including its probability mass function (PMF, $\mathsf{P}(\cdot)$) and cumulative distribution function (CDF, $\mathsf{F}(\cdot)$) for $\alpha > 0$ and $\mu > 1$ as follows:

$$\mathsf{P}(x;\boldsymbol{\theta}) = \mathsf{S}(x) - \mathsf{S}(x+1) = \exp\left(1-\mu^{x^\alpha}\right) - \exp\left(1-\mu^{(x+1)^\alpha}\right),\ x = 0, 1, 2, \ldots, \tag{2.4}$$

$$\mathsf{F}(x;\boldsymbol{\theta}) = \mathsf{P}(X \le x) = 1 - \mathsf{S}(x) + \mathsf{P}(X = x) = 1 - \exp\left(1-\mu^{(x+1)^\alpha}\right),\ x = 0, 1, 2, \ldots, \tag{2.5}$$

respectively.

It is worth noting here that the continuous Pham's CDF $G(\cdot)$ in (2.2) leads to the corresponding SF in (2.3). Because $\mathsf{S}(0) = 1$, this SF can be directly discretized without normalization by defining $\mathsf{P}(X = x) = \mathsf{S}(x) - \mathsf{S}(x+1)$, yielding a valid discrete distribution. The PMF (2.4) of the DPham distribution exhibits high flexibility, allowing decreasing, increasing, or unimodal shapes depending on the interaction between the power shape parameter α and the scale parameter μ (see Theorem 1).

Theorem 1. *Let $X \sim$ DPham($\boldsymbol{\theta}$) with parameters $\alpha > 0$ and $\mu > 1$; then, its PMF satisfies the following shapes:*

(1) For $0 < \alpha \leq 1$, the PMF $\mathsf{P}(x)$ is monotonically decreasing in x;
(2) For $\alpha > 1$, the PMF is initially increasing in x for small values of x;
(3) For α ($\to$ large) and $\mu \to 1$, the PMF is unimodal, that is it increases up to some mode and decreases thereafter.

Proof. See Appendix 1. □

Figure 1 depicts six panels that illustrate the behavioral patterns of the PMF (2.4) depending on the parameter combinations of α and μ. It exhibits that the PMF (2.4) can be decreasing (for $0 < \alpha \leq 1$ and $\mu > 1$), increasing (for $\alpha > 1$), or unimodal (for $\alpha \gg 1$ and $\mu \gtrsim 1$) shapes, depending on α. It also exhibits stepwise, bounded behavior, reflecting the inherent discreteness of the distribution.

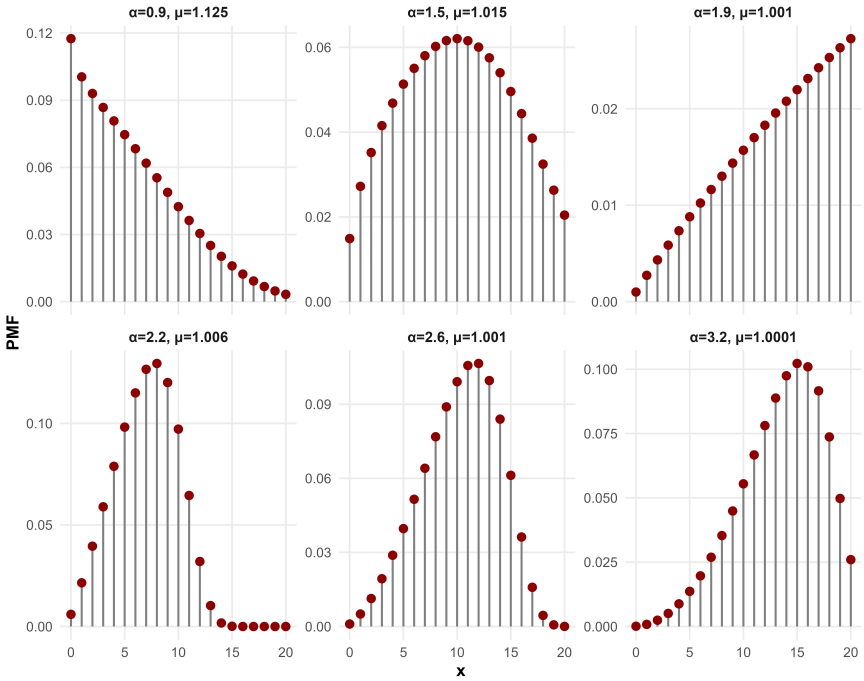

Figure 1. The PMF shapes of the DPham distribution.

3. Statistical functions

This section discusses several statistical functions for the DPham distribution, including the hazard rate, quantile, moments, and order statistics.

3.1. Hazard rate

Consider X is a DPham random variable, denoted by $X \sim$ DPham($\boldsymbol{\theta}$), with parameters $\alpha > 0$ and $\mu > 1$. Then, the corresponding hazard rate function (HRF) (say, $\mathsf{h}(\cdot)$) is

$$\mathsf{h}(x;\boldsymbol{\theta}) = \frac{\mathsf{P}(x)}{\mathsf{S}(x)} = 1 - \exp\left(\mu^{x^\alpha} - \mu^{(x+1)^\alpha}\right). \tag{3.1}$$

It is worth noticing here that the HRF (3.1) of the DPham distribution is flexible and capable of modeling increasing, constant, and bathtub-shaped aging behaviors (see Theorem 2). This versatility is driven by the convexity properties of the operator μ^{x^α}, which governs the discrete increments of the survival function.

Theorem 2. *Let X be a discrete, random variable following the DPham distribution, denoted by $X \sim$ DPham($\boldsymbol{\theta}$). Then, its HRF satisfies the following properties:*

(i) $h(x)$ *is increasing for* $\alpha > 1$*;*
(ii) $h(x)$ *is constant for* $\alpha = 1$*;*
(iii) $h(x)$ *is a V-tub bathtub-shaped for* $0 < \alpha < 1$.

Proof. See Appendix 2. □

Figure 2 exhibits that the HRF (3.1) can be bathtub-shaped (V-tub) (for $0 < \alpha < 1$); monotone increasing (for $\alpha > 1$), or constant (for $\alpha = 1$ and $\mu \to 1$). Hence, the DPham successfully mirrors the hazard flexibility of the continuous Pham distribution, including V-tub-shaped, increasing, and constant patterns. It is highly flexible, able to model various shapes in count/lifetime data, mirroring the continuous version's versatility. Overall, these properties demonstrate that the DPham distribution effectively preserves the key flexibility of the continuous Pham distribution while adapting it for discrete lifetime or count data applications.

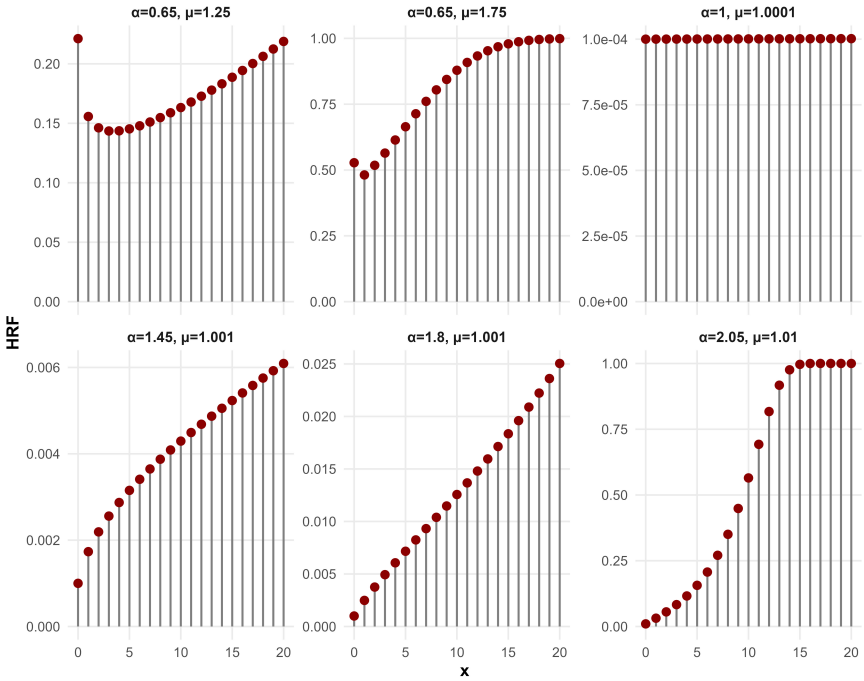

Figure 2. The HRF shapes of the DPham distribution.

3.2. Quantile

For a discrete distribution, the inverse of the CDF corresponds to the quantile function, denoted by $\mathsf{Q}(u)$. This function is primarily employed in simulation studies to generate random variates.

Theorem 3. *Let X be a DPham random variable having a CDF (2.5); then, for $0 < u < 1$, the corresponding quantile function $Q(u) = F^{-1}(u; \boldsymbol{\theta})$ has*

$$Q(u; \boldsymbol{\theta}) = \left[\frac{\ln(1 - \ln(1-u))}{\ln(\mu)} \right]^{\frac{1}{\alpha}} - 1, \quad 0 < u < 1, \tag{3.2}$$

expressed in the linear closed-form solution.

Proof. See Appendix 3. □

3.3. Moments and related measures

This part develops and evaluates the moments of the DPham model and its associated measures, including the coefficient of variation, skewness, and kurtosis, among others. Let X be a nonnegative, discrete, random variable with PMF (2.4); then, for any integer $r \geq 1$, the rth raw moment of X (say, $\mathcal{M}^r$) is given by

$$\mathbb{E}(X^r) = \sum_{x=0}^{\infty} x^r \mathsf{P}(x; \boldsymbol{\theta}) = \sum_{x=0}^{\infty} x^r \left[\exp(1 - \mu^{x^\alpha}) - \exp(1 - \mu^{(x+1)^\alpha}) \right]. \tag{3.3}$$

Applying the discrete summation-by-parts identity,

$$\sum_{x=0}^{\infty} a_x (b_x - b_{x+1}) = \sum_{x=0}^{\infty} b_{x+1} (a_{x+1} - a_x),$$

with $a_x = x^r$ and $b_x = \mathsf{S}(x; \boldsymbol{\theta})$. We re-express (3.3) as

$$\sum_{x=0}^{\infty} x^r \left[\exp(1 - \mu^{x^\alpha}) - \exp(1 - \mu^{(x+1)^\alpha}) \right] = \sum_{x=0}^{\infty} \exp(1 - \mu^{(x+1)^\alpha}) \left[(x+1)^r - x^r \right]. \tag{3.4}$$

As a result, for a nonnegative, integer-valued X that follows the DPham model, the rth raw moment is

$$\mathcal{M}^r = \sum_{x=0}^{\infty} \exp(1 - \mu^{(x+1)^\alpha}) \left[(x+1)^r - x^r \right]. \tag{3.5}$$

Remark 1. *Closed-form expressions for rth moments are generally not available. However, the above series representation allows accurate numerical evaluation of the moments and facilitates the derivation of special cases such as the mean ($r = 1$) and variance.*

Consequently, substituting $r = 1$ and 2 into (3.5), the first and second noncentral moments of X, respectively, are

$$\mathcal{M} = \sum_{x=0}^{\infty} \exp(1 - \mu^{(x+1)^\alpha}), \tag{3.6}$$

and

$$\mathcal{M}^2 = \sum_{x=0}^{\infty} x^2 \exp(1 - \mu^{(x+1)^\alpha}). \tag{3.7}$$

Further, from (3.6) and (3.7), the DPham distribution's variance (say, $\mathcal{V}$) is

$$\mathcal{V} = \sum_{x=0}^{\infty} x^2 \exp(1-\mu^{(x+1)^\alpha}) - \left[\sum_{x=0}^{\infty} \exp(1-\mu^{(x+1)^\alpha})\right]^2. \tag{3.8}$$

When comparing the variability of two independent samples, the coefficient of variation ($\mathcal{CV}$) serves as a natural and informative measure, as it quantifies dispersion on a relative scale. The $\mathcal{CV}$ is especially appealing due to its dimensionless and scale-invariant nature, enabling meaningful comparisons of variability across datasets that differ in magnitude or measurement units. Mathematically, we formulate $\mathcal{CV}$ as follows:

$$\mathcal{CV} = \frac{\mathcal{V}^{0.5}}{\mathcal{M}} = \frac{\sqrt{\sum_{x=0}^{\infty} x^2 \exp(1-\mu^{(x+1)^\alpha}) - \left[\sum_{x=0}^{\infty} \exp(1-\mu^{(x+1)^\alpha})\right]^2}}{\sum_{x=0}^{\infty} \exp(1-\mu^{(x+1)^\alpha})}.$$

Additionally, the variance-to-mean ratio (or dispersion index) ($\mathcal{DI}$) is given by

$$\mathcal{DI} = \frac{\mathcal{V}}{\mathcal{M}}. \tag{3.9}$$

In contrast to $\mathcal{CV}$, the $\mathcal{DI}$ is not scale-invariant and is primarily used for modeling non-negative, discrete data. It is a fundamental diagnostic measure in count data analysis, as it quantifies departures from the equidispersion property inherent to the Poisson distribution. Specifically,

- $\mathcal{DI} > 1$: indicates *overdispersion*, where the variability lies over the Poisson benchmark;
- $\mathcal{DI} = 1$: indicates *equidispersion*, corresponding to the Poisson case;
- $\mathcal{DI} < 1$: indicates *underdispersion*, where the variability is smaller than expected.

Using the cumulants, denoted by C_r, the coefficients of skewness and kurtosis can be derived from the ordinary moments of the random variable X. When X follows a DPham($\boldsymbol{\theta}$) distribution, the first four cumulants of X are given by

$$C_r = \mathcal{M}^r - \sum_{i=0}^{r-1} \binom{r-1}{i-1} C_i \mathcal{M}^{r-i}. \tag{3.10}$$

Once C_r (for $r = 2, 3, 4$) obtained, the corresponding coefficients of skewness (say, Φ_s), and kurtosis (say, Φ_k), of DPham distribution can easily be obtained, as follows:

$$\Phi_s = C_3/C_2^{3/2}, \quad \text{and} \quad \Phi_k = C_4/C_2^2,$$

respectively.

In Table 1, a comprehensive numerical analysis about six measures ($\mathcal{M}$, $\mathcal{V}$, $\mathcal{DI}$, $\mathcal{CV}$, Φ_s, Φ_k) for various options of α and μ is summarized. As α (or μ) grows, the results in Table 1 show:

- For $\mathcal{M}$: It decreases systematically as μ increases (for fixed α), indicating that larger values of μ shift probability mass toward smaller counts; additionally, increasing α accelerates this decay, reflecting stronger concentration around lower support values.

- For $\mathcal{V}$: It exhibits a similar decreasing trend with respect to μ while remaining relatively large for small α, demonstrating that the distribution is capable of modeling highly variable count data and gradually transitions to more concentrated behavior as parameters increase.
- For $\mathcal{ID}$: It exceeds unity for most parameter combinations, confirming the ability of the DPham distribution to accommodate overdispersed data, whereas values approaching one for larger α suggest convergence toward equidispersion under specific regimes;
- For $\mathcal{CV}$: It remains generally above one across a wide parameter range, indicating substantial relative variability; its increase for larger μ highlights the model's flexibility in capturing heterogeneity even when the mean is small.
- For Φ_s: It dominates most parameter settings, implying a right-tailed distribution suitable for modeling rare but extreme events, whereas the reduction or sign change at higher α values reflects increasing symmetry as the distribution becomes more concentrated.
- For Φ_k: It exceeds the Gaussian benchmark, indicating heavy-tailed behavior and strong peakness, which underscores the suitability of the DPham distribution for data exhibiting extreme variability and outlier-prone behavior.

Collectively, these six measures demonstrate that the DPham distribution provides substantial flexibility in location, dispersion, and shape, enabling it to model a wide spectrum of discrete lifetime and count data structures encountered in reliability and applied statistical contexts. Figure 3 visualizes the actual behavior of $\mathcal{M}$, $\mathcal{V}$, Φ_s, and Φ_k and supports the numerical findings in Table 1.

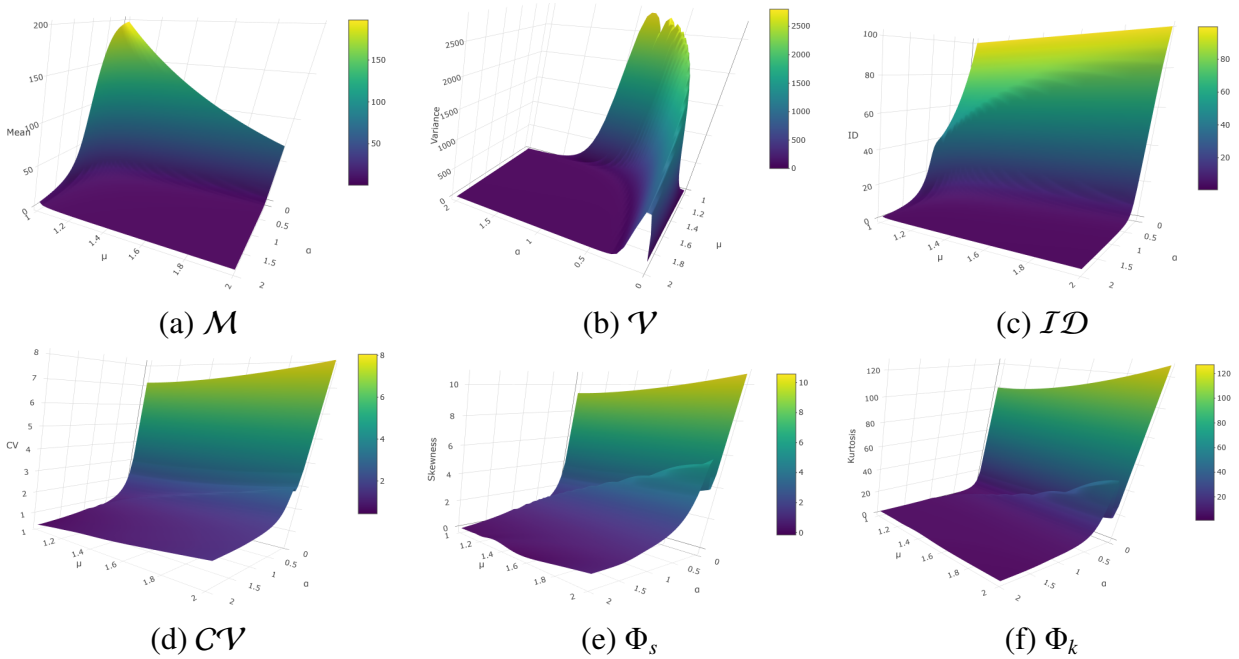

(a) $\mathcal{M}$ (b) $\mathcal{V}$ (c) $\mathcal{ID}$

(d) $\mathcal{CV}$ (e) Φ_s (f) Φ_k

Figure 3. Distributional shapes of the DPham model.

Table 1. Outputs of six distributional measures of the DPham($\boldsymbol{\theta}$).

μ	$\mathcal{M}$	$\mathcal{V}$	$\mathcal{ID}$	$\mathcal{CV}$	Φ_s	Φ_k
$\alpha = 0.5$						
1.1	4.6747	25.726	9.6180	1.2295	1.9439	5.6533
1.3	2.3229	28.250	6.5351	1.3701	1.2465	3.5484
1.5	1.7132	13.818	5.0930	1.7321	1.8287	6.3320
2.0	0.7498	1.6866	2.2495	1.8963	2.3399	9.7414
2.5	0.3206	0.4838	1.5090	2.1694	2.6624	11.486
$\alpha = 1.0$						
1.1	2.7286	19.015	3.3193	0.7612	0.6835	2.8193
1.3	1.7949	2.5446	1.4177	0.8887	0.7678	3.0210
1.5	1.0047	1.0549	1.0500	1.0223	0.8388	3.0801
2.0	0.4186	0.3466	0.8280	1.4065	1.1035	3.3462
2.5	0.2284	0.1867	0.8176	1.8921	1.4877	3.7595
$\alpha = 1.5$						
1.1	2.6887	2.7111	1.0083	0.6124	0.2228	1.5092
1.3	1.1289	0.7428	0.7769	0.7635	0.2823	2.3024
1.5	0.7240	0.4362	0.6580	0.9122	0.3838	2.3434
2.0	0.3701	0.2376	0.6420	1.3170	0.5959	2.3773
2.5	0.2231	0.1734	0.6025	1.8660	1.3302	2.7699
$\alpha = 2.0$						
1.1	1.8182	0.9636	0.7769	0.5399	0.0588	1.3003
1.3	0.8972	0.4051	0.6321	0.7094	0.0916	1.8379
1.5	0.6237	0.2691	0.5300	0.8317	0.1378	2.4112
2.0	0.3679	0.2325	0.4515	1.3108	0.5480	2.4399
2.5	0.2231	0.1733	0.4314	1.8659	1.3300	2.7689

3.4. Order statistics

Consider $(X_1, X_2, \ldots, X_n)$ an identical random sample drawn from the DPham model, and let $(X_1^\star, X_2^\star, \ldots, X_n^\star)$ represent the corresponding order statistics. Then, the CDF of the ith-order statistic is given by

$$\mathsf{F}_{i:n}(x;\boldsymbol{\theta}) = \sum_{j=i}^{n} \binom{n}{j} [\mathsf{F}(x_i^\star;\boldsymbol{\theta})]^j [\mathsf{S}(x_i^\star;\boldsymbol{\theta})]^{n-j}. \tag{3.11}$$

The CDF (3.11) can be expanded into a series by applying the negative binomial theorem, which is expressed as

$$\mathsf{F}_{i:n}(x;\boldsymbol{\theta}) = \sum_{j=i}^{n} \sum_{k=1}^{n-j} \binom{n}{j} \binom{n-j}{k} (-1)^k [\mathsf{F}(x_i^\star;\boldsymbol{\theta})]^{j+k}. \tag{3.12}$$

So, from (2.5), the CDF (3.12) of the ith-order statistic becomes

$$\mathsf{F}_{i:n}(x;\boldsymbol{\theta}) = \sum_{j=i}^{n} \sum_{k=1}^{n-j} \binom{n}{j} \binom{n-j}{k} (-1)^k [1 - \exp(1 - \mu^{(x_i^\star+1)^\alpha})]^{j+k}. \tag{3.13}$$

Correspondingly, the PMF of the ith-order statistic is given by

$$\mathsf{P}_{i:n}(x;\boldsymbol{\theta}) = \sum_{j=i}^{n}\sum_{k=1}^{n-j}\binom{n}{j}\binom{n-j}{k}(-1)^k[\exp(1-\mu^{x^\alpha}) - \exp(1-\mu^{(x+1)^\alpha})]^{j+k}. \tag{3.14}$$

Moreover, following (3.14), the rth moment of the $X^\star_{i:n}$-order statistic can be easily formulated as follows:

$$\mathbb{E}(X^r_{i:n}) = \sum_{i=1}^{\infty}\sum_{j=i}^{n}\sum_{k=1}^{n-j}\binom{n}{j}\binom{n-j}{k}(-1)^k[\exp(1-\mu^{x^\alpha}) - \exp(1-\mu^{(x+1)^\alpha})]^{j+k}. \tag{3.15}$$

Order statistics play a crucial role in characterizing the behavior of a distribution at its extremes. To investigate the tail behavior, we focus on the minimum and maximum order statistics, corresponding to $i = 1$ and n in (3.14). These statistics provide valuable insights into early failures and long-lived components, respectively, which are particularly relevant in reliability studies. From (3.14), simplified expressions for the minimum and maximum order statistics can be derived, respectively, as follows:

- The PMF of the minimum order statistic, $X^\star_1$:

$$\mathsf{P}(x^\star_1;\boldsymbol{\theta}) = [\mathsf{S}(x-1;\boldsymbol{\theta})]^n - [1-\mathsf{S}(x;\boldsymbol{\theta})]^n = e^{n[1-\mu^{x^\alpha}]}\left[e^{n[\mu^{x^\alpha}-\mu^{(x-1)^\alpha}]} - 1\right].$$

- The PMF of the maximum order statistic, $X^\star_n$:

$$\mathsf{P}(x^\star_n;\boldsymbol{\theta}) = [\mathsf{F}(x;\boldsymbol{\theta})]^n - [\mathsf{F}(x-1;\boldsymbol{\theta})]^n = \left[1-e^{1-\mu^{x^\alpha}}\right]^n - \left[1-e^{1-\mu^{(x-1)^\alpha}}\right]^n.$$

To examine the tail behavior of the DPham($\boldsymbol{\theta}$) distribution, using different configurations of sample size $n \in (5, 10, 20, 50, 100)$, $\alpha \in (0.5, 1.0, 1.5)$, and $\mu \in (1.1, 1.5, 2.0, 2.5)$, numerical evaluations of the minimum and maximum, $\mathbb{E}[X^\star_1]$ and $\mathbb{E}[X^\star_n]$ are reported in Table 2. For instance, a value of 2.75E-02 corresponds to 2.75×10^{-2}.

Table 2 lists the following key observations:

- The expected minimum $\mathbb{E}[X^\star_1]$ decreases rapidly as n increases, confirming the strong lower-tail concentration of the proposed distribution. This decay is particularly pronounced for larger values of the shape parameter α.
- For fixed n, increasing μ leads to an exponential reduction in $\mathbb{E}[X^\star_1]$, often driving the minimum to values numerically indistinguishable from zero even for moderate n.
- The expected maximum $\mathbb{E}[X^\star_n]$ exhibits a markedly different behavior, showing substantial growth with n when $\mu \to 1$, which indicates the presence of heavy upper tails in this regime.
- As μ increases, the growth of $\mathbb{E}[X^\star_n]$ is progressively dampened, and for large μ, the maximum stabilizes around moderate values regardless of n.
- Increasing α consistently reduces $\mathbb{E}[X^\star_n]$, demonstrating that α acts as a tail-thinning parameter that controls the extremal variability of the distribution.
- The joint effect of (α, μ) produces highly asymmetric extremes, where the minimum collapses rapidly while the maximum may remain large, especially for small α and μ close to one.
- These results highlight a strong interaction between distributional parameters and sample size, implying that inference-based on order statistics must explicitly account for (α, μ, n) to avoid misleading conclusions.

Overall, the DPham distribution exhibits rich and flexible extremal behavior, making it suitable for modeling data characterized by frequent near-zero observations coexisting with potentially large extreme values. Heatmap visualization tools, displayed in Figure 4, confirm all results presented in Table 2.

Table 2. Summary of $\mathbb{E}[X_1^\star]$ (1^{st} col.) and $\mathbb{E}[X_n^\star]$ (2^{nd} col.) using various options of α and μ.

n	$\mu\downarrow$ $\alpha\rightarrow$	0.5		1		1.5	
5	1.1	1.37E+00	2.10E-02	7.21E-01	3.41E+00	2.57E-01	4.64E+00
	1.5	2.98E-02	4.12E+00	1.94E-03	2.28E+00	2.16E-05	1.46E+00
	2.0	2.52E-04	2.39E+00	3.06E-07	1.13E+00	5.59E-14	9.10E-01
	2.5	1.73E-06	1.15E+00	3.98E-12	7.43E-01	1.51E-27	7.17E-01
10	1.1	1.03E-05	2.31E-40	7.58E-10	3.94E-07	3.65E-14	6.59E+00
	1.5	2.35E-34	2.34E-02	5.17E-55	3.95E+00	5.07E-94	2.07E+00
	2.0	4.83E-73	6.20E+00	5.1E-131	2.08E+00	8.9E-186	1.20E+00
	2.5	5.5E-116	3.42E+00	9.9E-229	1.41E+00	8.9E-266	1.00E+00
20	1.1	6.83E-01	7.15E-05	1.71E-01	1.63E+00	4.70E-02	5.24E+00
	1.5	4.76E-04	3.88E+00	3.73E-06	2.76E+00	4.68E-10	1.72E+00
	2.0	5.87E-08	3.31E+00	9.36E-14	1.40E+00	3.13E-27	1.01E+00
	2.5	2.98E-12	1.69E+00	1.58E-23	9.71E-01	2.27E-54	9.20E-01
50	1.1	1.16E-01	6.52E-10	1.64E-02	3.17E-01	2.06E-03	5.73E+00
	1.5	1.90E-07	2.48E+00	1.39E-11	3.18E+00	2.19E-19	1.93E+00
	2.0	3.44E-15	4.24E+00	8.76E-27	1.66E+00	9.77E-54	1.04E+00
	2.5	8.86E-24	2.23E+00	2.51E-46	1.09E+00	5.2E-108	9.94E-01
100	1.1	9.00E-04	3.96E-25	2.76E-05	1.97E-03	1.91E-07	6.26E+00
	1.5	1.53E-17	4.57E-01	7.19E-28	3.64E+00	2.25E-47	2.03E+00
	2.0	6.95E-37	5.40E+00	7.18E-66	1.97E+00	3.0E-133	1.11E+00
	2.5	2.34E-58	2.92E+00	9.9E-115	1.23E+00	6.0E-269	1.00E+00

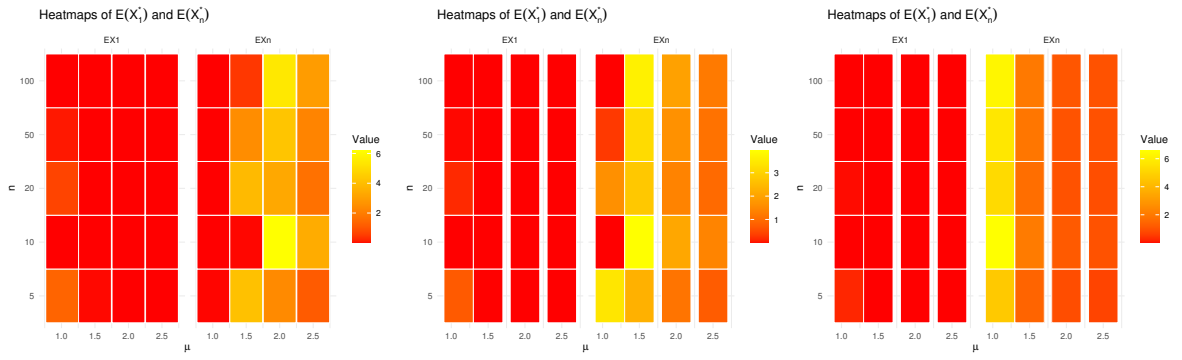

(a) $\alpha = 0.5$ (b) $\alpha = 1$ (c) $\alpha = 1.5$

Figure 4. Heatmaps for the $\mathbb{E}[X_1^\star]$ and $\mathbb{E}[X_n^\star]$ order statistics using various options of the DPham parameters.

4. Parametric inference

This section derives the MLE $\hat{\boldsymbol{\theta}}$ of $\boldsymbol{\theta}$ using a dataset collected by the CT2 strategy. According to this sampling plan, the experiment is terminated after a prespecified number of failures, say r, is observed. At the same time, the remaining surviving units, $n - r$, are treated as censored observations. It also provides a simpler experimental design and yields a more tractable LF, which is advantageous when working with flexible, potentially intricate lifetime distributions. Let $\mathbf{x} = (x_{1:n}, x_{2:n}, \ldots, x_{r:n})$ denote a CT2 sample drawn from the DPham($\boldsymbol{\theta}$) distribution. We now define the LF (say, $\mathsf{L}(\cdot)$) of such censored data as

$$\mathsf{L}(\boldsymbol{\theta}|\mathbf{x}) \propto \prod_{i=1}^{r} \mathsf{P}(x_{i:n})[\mathsf{S}(x_{i:n};\boldsymbol{\theta})]^{n-r}. \tag{4.1}$$

4.1. Likelihood estimation

Substituting the PMF (2.4) and CDF (2.5) into the LF (4.1), the LF, denoted by $\mathsf{L}(\cdot)$, and the corresponding log-LF, denoted by $\mathsf{L}^{\star}(\cdot)$, can be formulated, respectively, as follows:

$$\mathsf{L}(\boldsymbol{\theta}|\mathbf{x}) \propto \prod_{i=1}^{r} \left[\exp(1-\mu^{x_i^{\alpha}}) - \exp(1-\mu^{(x_i+1)^{\alpha}})\right] e^{(n-r)[1-\mu^{(x_r+1)^{\alpha}}]}, \tag{4.2}$$

and

$$\mathsf{L}^{\star}(\boldsymbol{\theta}|\mathbf{x}) \propto \sum_{i=1}^{r} \log\left[\exp(1-\mu^{x_i^{\alpha}}) - \exp(1-\mu^{(x_i+1)^{\alpha}})\right] + (n-r)[1-\mu^{(x_r+1)^{\alpha}}], \tag{4.3}$$

respectively, where $x_i \to x_{i:n}$ (for simplicity).

Differentiating (4.3) partially with respect to α and μ yields the MLEs of α and μ (symbolized by $\hat{\alpha}$ and $\hat{\mu}$, respectively). The respective score equations of α and μ, from (4.3), are as follows:

$$\sum_{i=1}^{r}\left[\frac{\zeta^{\circ}(x_i+1;\alpha,\mu) - \zeta^{\circ}(x_i;\alpha,\mu)}{\zeta(x_i;\alpha,\mu)}\right] + (n-r)\,\zeta^{\circ}(x_r+1;\alpha,\mu)\Big|_{(\hat{\alpha},\hat{\mu})} = 0, \tag{4.4}$$

and

$$\sum_{i=1}^{r}\left[\frac{\zeta^{\bullet}(x_i+1;\alpha,\mu) - \zeta^{\bullet}(x_i;\alpha,\mu)}{\zeta(x_i;\alpha,\mu)}\right] + (n-r)\,\zeta^{\bullet}(x_r+1;\alpha,\mu)\Big|_{(\hat{\alpha},\hat{\mu})} = 0, \tag{4.5}$$

where $\zeta(x_i;\alpha,\mu) = e^{\mu^{x_i^{\alpha}} - \mu^{(x_i+1)^{\alpha}}}$, $\zeta^{\circ}(j;\alpha,\mu) = j^{\alpha}\log(j)\log(\mu)\mu^{j^{\alpha}}\exp\left(1-\mu^{j^{\alpha}}\right)$, and $\zeta^{\bullet}(j;\alpha,\mu) = j^{\alpha}\mu^{j^{\alpha}-1}\exp\left(1-\mu^{j^{\alpha}}\right)$ (for $j = x_i, x_i+1$).

Remark 2. *The score Eqs (4.4) and (4.5) of α and μ, respectively, do not admit closed-form solutions for their MLEs, and hence, iterative procedures such as the Newton-Raphson (NR) algorithm are employed to obtain $\hat{\alpha}$ and $\hat{\mu}$.*

To ensure that the parameter constraint $\mu \in (1,\infty)$ is satisfied throughout the iterative process, we adopt the reparameterization $\mu = 1 + \exp(\eta)$, where $\eta \in \mathbb{R}$. The NR algorithm is then implemented on the transformed parameter η, which allows unconstrained optimization while guaranteeing that all updated values of μ automatically satisfy $\mu > 1$.

Importantly, this reparameterization does not alter any analytical expressions of the DPham model; it only modifies the estimation procedure to enforce $\mu > 1$ and improve numerical stability. Accordingly, the updating scheme for α (for $\iota = 0, 1, 2, \ldots$) is given by

$$\alpha^{(\iota+1)} = \alpha^{(\iota)} - \frac{\mathcal{S}_\alpha(\alpha^{(\iota)}, \eta^{(\iota)})}{\mathcal{H}_\alpha(\alpha^{(\iota)}, \eta^{(\iota)})},$$

whereas for η,

$$\eta^{(\iota+1)} = \eta^{(\iota)} - \frac{\mathcal{S}_\eta(\alpha^{(\iota)}, \eta^{(\iota)})}{\mathcal{H}_\eta(\alpha^{(\iota)}, \eta^{(\iota)})}.$$

Here, $\mathcal{S}_\alpha$ and $\mathcal{S}_\eta$ denote the score functions, and $\mathcal{H}_\alpha$ and $\mathcal{H}_\eta$ are the corresponding observed information quantities. The sequence $\{\eta^{(\iota)}\}$ induces $\{\mu^{(\iota)}\}$ through the transformation $\mu^{(\iota)} = 1 + \exp(\eta^{(\iota)})$, ensuring that the constraint is preserved at every iteration.

The iterative procedure is continued until convergence criteria based on successive parameter updates and log-LF increments are satisfied. In practice, we recommend implementing the NR algorithm using the maxLik package (by Henningsen and Toomet [22]) via the $\mathcal{R}$ programming platform, which provides robust tools for LF-maximization.

To investigate the existence and uniqueness of the MLEs $\hat{\alpha}$ and $\hat{\mu}$, owing to the complicated structures of their score equations in (4.4) and (4.5), respectively, see Figure 5. It is created from DPham(0.5, 1.2) (as an example) when $(n, r) = (80, 40)$, and the MLE values of $\hat{\alpha}$ and $\hat{\mu}$ are 0.5324 and 1.2727, respectively. The log-LF for both parameters appears unimodal, the score functions exhibit a unique zero-crossing, and the observed information remains negative in a neighborhood of the optimum. These features indicate local concavity and hence stability of the NR updates when initialized reasonably close to the maximum likelihood estimates. Nevertheless, numerical instability may arise when initial values are far from the optimum or when the observed information is close to zero. To handle such issues and to ensure reliable convergence in practical applications, we recommend the use of quasi-Newton optimization (e.g., Broyden-Fletcher-Goldfarb-Shanno (BFGS)) methods available in the maxLik package.

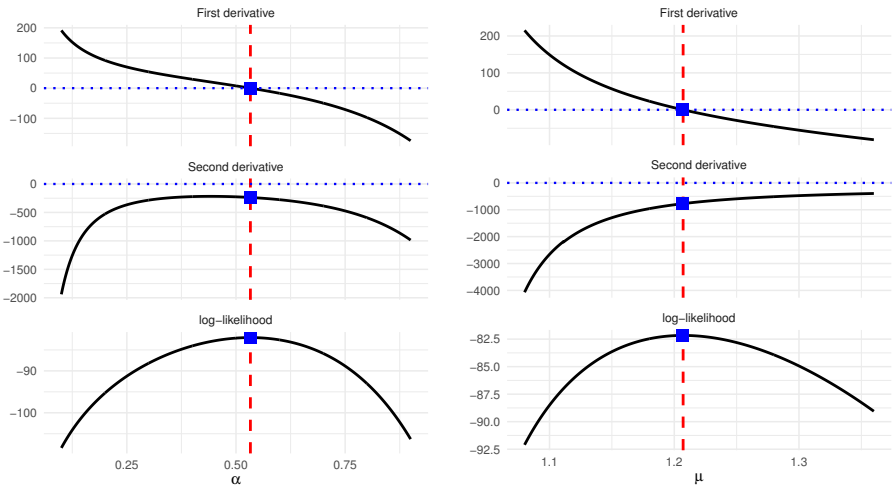

Figure 5. The existence and uniqueness of α and μ.

Theorem 4. *Consider $L^{\star}(\boldsymbol{\theta}|\boldsymbol{x})$, where $(\boldsymbol{x})$ represents the observed CT2 failure times, and $(\boldsymbol{\theta})$ denotes the fixed parameter vector. This expression pertains to the DPham log-LF using Type-II censoring. The MLEs $\hat{\alpha}$ and $\hat{\mu}$ are, then,*

$$(\hat{\alpha}, \hat{\mu}) = \arg\max_{(\alpha,\mu)\in\boldsymbol{\theta}} L^{\star}(\boldsymbol{\theta}|\boldsymbol{x});$$

they exist and are unique.

Proof. See Appendix 4. □

4.2. Bayesian estimation

This section addresses the Bayesian estimation of the parameters $(\boldsymbol{\theta})$ of the DPham model. Following this framework, the parameters α and μ are treated as random variables following the gamma prior distributions, characterized by the non-negative hyperparameters (a, b) for α and (c, d) for μ. In the absence of reliable prior information, the choice of an appropriate prior becomes particularly important. The joint priori PDF for $(\boldsymbol{\theta})$, say $\phi(\cdot)$, is

$$\phi(\boldsymbol{\theta}) \propto \alpha^{a-1}(\mu-1)^{c-1}e^{-(b\alpha+d(\mu-1))},\ a,b,c,d>0,\ \alpha>0,\ \mu>1, \tag{4.6}$$

where (a, b, c, d) denote the non-negative hyperparameters.

Given the information gathered by the sample data (4.2) and prior knowledge (4.6), the posterior probability density function (PDF) of $(\boldsymbol{\theta})$, say $\psi(\cdot)$, is given by

$$\psi(\boldsymbol{\theta}|\mathbf{x}) = \Xi^{-1}\mathsf{L}(\boldsymbol{\theta}|\mathbf{x})\phi(\boldsymbol{\theta}), \tag{4.7}$$

where $\Xi(=\int_{\theta}\mathsf{L}(\boldsymbol{\theta}|\mathbf{x})\phi(\boldsymbol{\theta}))$ is the normalized term that is free of parameters.

From (4.2) and (4.6), we can re-express (4.7) as follows:

$$\psi(\boldsymbol{\theta}|\mathbf{x}) = \Xi^{-1}\alpha^{a-1}(\mu-1)^{c-1}e^{-(b\alpha+d(\mu-1))}e^{(n-r)[1-\mu^{(x_r+1)^{\alpha}}]}\times\prod_{i=1}^{r}\left[\exp(1-\mu^{x_i^{\alpha}})-\exp(1-\mu^{(x_i+1)^{\alpha}})\right]. \tag{4.8}$$

A Bayesian estimate of the shape parameter α (for instance), say $\tilde{\alpha}$ from the squared error loss, is directly given by the expected value for the joint posterior PDF (4.7) as follows:

$$\tilde{\alpha} = \Xi^{-1}\int_{\alpha}\mathsf{L}(\boldsymbol{\theta}|\mathbf{x})\phi(\boldsymbol{\theta})\mathrm{d}\alpha. \tag{4.9}$$

Analytical forms for the Bayes estimators of α and μ are generally intractable, which makes numerical approximation unavoidable. Accordingly, the Bayesian estimation procedure relies on numerical integration techniques. In this regard, stochastic simulation methods within the Markov chain Monte Carlo (MCMC) framework are especially appropriate for approximating posterior summaries. For the parameter vector $\boldsymbol{\theta}$ and based on (4.7), the Bayesian framework proceeds by deriving the relevant conditional posterior PDFs of α and μ, such as

$$\psi^{\alpha}(\alpha|\mu,\mathbf{x}) \propto \alpha^{a-1}e^{-b\alpha}\mathsf{L}(\alpha,\mu|\mathbf{x}), \tag{4.10}$$

$$\psi^{\mu}(\mu|\alpha,\mathbf{x}) \propto (\mu-1)^{c-1}e^{-d(\mu-1)}\mathsf{L}(\alpha,\mu|\mathbf{x}), \tag{4.11}$$

respectively.

Based on (4.10) and (4.11), the Bayes estimators $\tilde{\alpha}$ and $\tilde{\mu}$ of α and μ, respectively, do not correspond to any standard probability distributions. To address this challenge, the Metropolis-Hastings (M-H) sampler, one of the foundational algorithms within the MCMC class of Bayesian computational methods, is employed. Unlike techniques that require conditional posteriors to belong to known distributional families, the M-H algorithm operates by generating candidate values from a proposal distribution and accepting or rejecting them according to a specified acceptance probability.

This mechanism ensures that the resulting Markov chain converges to the target posterior distribution. In this study, a normal distribution is adopted as the proposal density for all DPham parameters; the implementation follows the steps outlined in Algorithm 1. Numerically, to execute this process, we recommend installing the coda package (by Plummer et al. [23]) in the $\mathcal{R}$ programming platform.

Algorithm 1 The M-H Algorithm for α and μ

1: **Input:** Start with $i = 1$
2: **Input:** Observed CT2 sample $\mathbf{x}$
3: **Input:** Total number of Bayes iterations $\mathbb{X}$, burn-in size $\mathbb{X}^{\bullet}$, and remaining size $\bar{\mathbb{X}} = \mathbb{X} - \mathbb{X}^{\bullet}$
4: **Input:** Proposal normal density $\Lambda(\cdot)$
5: **Initialization:** Set initial values $(\alpha^{(0)}, \mu^{(0)})$
6: **for** $i = 1$ to $\mathbb{X}$ **do**
7: **Step 1: Proposal generation**
8: Draw $\alpha^{\star} \sim \Lambda_{\alpha}(\cdot \mid \alpha^{(i-1)})$
9: **Step 2: Acceptance ratio**

$$O_{\alpha} = \min\left\{1, \frac{\psi^{\alpha}(\alpha^{\star}|\bullet)\Lambda_{\alpha}(\alpha^{(i-1)} \mid \alpha^{\star})}{\psi^{\alpha}(\alpha^{(i-1)}|\bullet)\Lambda_{\alpha}(\alpha^{\star} \mid \alpha^{(i-1)})}\right\}.$$

10: **Step 3: Uniform variate**
11: Draw $u \sim \text{Uniform}(0, 1)$
12: **Step 4: Accept/reject**

$$\alpha^{(i)} = \begin{cases} \alpha^{\star}, & \text{if } u \leq \min(1, O_{\alpha}), \\ \alpha^{(i-1)}, & \text{otherwise.} \end{cases}$$

13: **end for**
14: **Output:** Posterior sample $\{\alpha^{(i)}\}_{i=\mathbb{X}^{\bullet}+1}^{\mathbb{X}}$
15: **Output:** Compute $\tilde{\alpha} = \frac{1}{\bar{\mathbb{X}}} \sum_{i=\mathbb{X}^{\bullet}+1}^{\mathbb{X}} \alpha^{(i)}$
16: **Repeat Steps 6–15** for μ

From DPham(0.5,1.2) and DPham(1.2,1.5), when $(n, r) = (100, 50)$, Figure 6 clearly indicates that the marginal posterior densities of both parameters α and μ are well-approximated by Gaussian distributions in the considered settings. For both DPham populations, the posterior curves almost perfectly overlap with their normal counterparts, suggesting strong posterior symmetry and negligible skewness. Conversely, using the same two DPham populations proposed, Figure 7 exhibits that the contours for both DPham populations are more symmetric and nearly elliptical, centered tightly around the posterior mode. The increased concentration of the contours further reflects higher posterior precision, consistent with the near-Gaussian marginal behavior observed in Figure 6. Collectively,

these figures demonstrate that the Bayesian posterior for the DPham model is well-behaved, with near-normal marginal distributions and interpretable joint dependence structures. Overall, although the posterior distributions of α and μ have no closed form, their conditional posteriors are smooth and approximately centered around the posterior mean. Consequently, the posterior distribution is well-approximated by a Gaussian density, which motivates the use of a random-walk M-H algorithm.

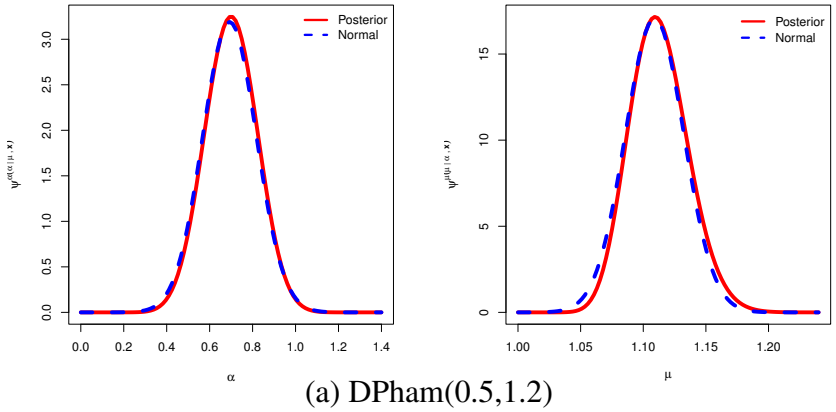

(a) DPham(0.5,1.2)

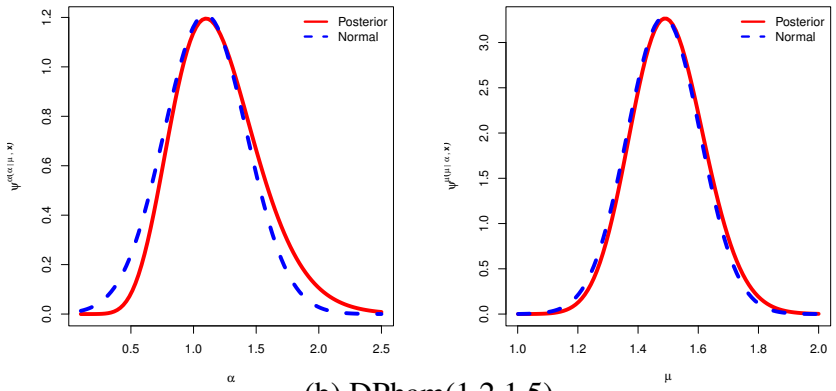

(b) DPham(1.2,1.5)

Figure 6. Posterior and Gaussian density shapes of α and μ.

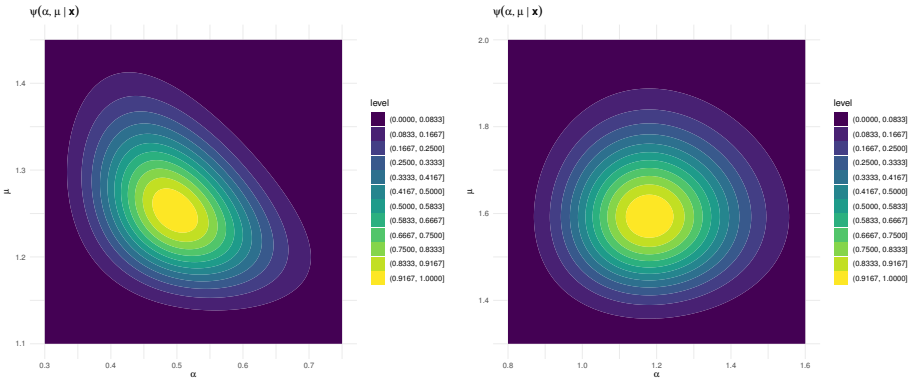

(a) DPham(0.5,1.2) (b) DPham(1.2,1.5)

Figure 7. Posterior contours of α and μ.

5. Interval inference

This section develops four interval estimation methodologies for the parameters of the DPham($\boldsymbol{\theta}$) model. Specifically, we consider two asymptotic confidence interval constructions and two Bayesian credible interval approaches. These methods stem from distinct inferential frameworks, classical

Fisher information inference, and Bayesian analysis, each differing in their underlying assumptions, theoretical motivation, and computational demands. The subsections that follow present the derivation of each procedure, outline the associated computational strategies, and clarify the interpretation of the resulting interval estimates.

5.1. Asymptotic method

To derive the $(1-v)100\%$ ACI under the normal approximation (ACI[NA]) for the DPham parameters $\boldsymbol{\theta}$, estimates of the variance of their MLEs, denoted by $\hat{\boldsymbol{\theta}}$, are required. To establish this, we differentiate (4.3) partially with respect to α and μ in turn to generate the Fisher information matrix (say, $\Sigma^{-1}(\cdot)$), whose inverse gives the covariances and variances (say, $\varepsilon_i,\ i=0,1,2$) of the DPham($\boldsymbol{\theta}$) model parameters (see Lawless [24]), such as

$$\widehat{\Sigma}^{-1}(\hat{\boldsymbol{\theta}}) = -\begin{pmatrix} \mathsf{L}_{11}^{\star} & \mathsf{L}_{12}^{\star} \\ \mathsf{L}_{21}^{\star} & \mathsf{L}_{22}^{\star} \end{pmatrix}_{(\boldsymbol{\theta}=\hat{\boldsymbol{\theta}})}, \tag{5.1}$$

where (for $j = x_i, x_i+1$) $\zeta^{\circ\circ}(j;\alpha,\mu) = \log(j)\,\zeta^{\circ}(j;\alpha,\mu)\left[1+\log(\mu)\left(1-\mu^{j^{\alpha}}\right)\right]$, $\zeta^{\bullet\bullet}(j;\alpha,\mu) = \mu^{-1}\zeta^{\bullet}(j;\alpha,\mu)\left[j^{\alpha}\left(1-\mu^{j^{\alpha}}\right)-1\right]$ and $\zeta^{\circ\bullet}(j;\alpha,\mu) = \log(j)\,\zeta^{\bullet}(j;\alpha,\mu)\left[1+j^{\alpha}\log(\mu)\left(1-\mu^{j^{\alpha}}\right)\right]$.

Then, the asymptotic variance matrix (say, $\Sigma(\cdot)$) of the MLEs of $\boldsymbol{\theta}$ is constructed as follows:

$$\widehat{\Sigma}(\hat{\boldsymbol{\theta}}) = \begin{pmatrix} \varepsilon_1 & \varepsilon_0 \\ \varepsilon_0 & \varepsilon_2 \end{pmatrix}_{(\boldsymbol{\theta}=\hat{\boldsymbol{\theta}})}. \tag{5.2}$$

Using (5.2), the $(1-v)100\%$ ACI[NA] estimators for α and μ can be formulated as follows:

$$\left(\hat{\alpha} - z_{0.5v}\sqrt{\hat{\varepsilon}_1}, \hat{\alpha} + z_{0.5v}\sqrt{\hat{\varepsilon}_1}\right),$$

and

$$\left(\hat{\mu} - z_{0.5v}\sqrt{\hat{\varepsilon}_2}, \hat{\mu} + z_{0.5v}\sqrt{\hat{\varepsilon}_2}\right),$$

respectively, where $z_{0.5v}$ denotes the upper $0.5v$-quantile of the standard normal distribution.

One of the drawbacks of the common ACI[NA] method is that it may produce a negative lower bound, even though the parameters $\alpha > 0$ and $\mu > 1$ are inherently constrained to be positive. In practical applications, these negative limits are often truncated at zero; however, this practice is improvised and lacks formal, reasoned justification. To address this issue and improve the robustness of interval estimation, Meeker and Escobar [25] advocated the use of the $(1-v)100\%$ ACI based on the normal approximation applied to the log-transformed parameter; this approach is known as ACI[NL]. Accordingly, the $(1-v)100\%$ ACI[NL] estimators for α and μ can be formulated as follows:

$$\left(\hat{\alpha}\exp\left(-z_{0.5v}\hat{\alpha}^{-1}\sqrt{\hat{\varepsilon}_1}\right), \hat{\alpha}\exp\left(+z_{0.5v}\hat{\alpha}^{-1}\sqrt{\hat{\varepsilon}_1}\right)\right),$$

and

$$\left(\hat{\mu}\exp\left(-z_{0.5v}\hat{\mu}^{-1}\sqrt{\hat{\varepsilon}_2}\right), \hat{\mu}\exp\left(+z_{0.5v}\hat{\mu}^{-1}\sqrt{\hat{\varepsilon}_2}\right)\right),$$

respectively.

5.2. Credible intervals

Within the Bayesian framework, two widely used interval estimation methods are implemented via MCMC simulations. The first is the BCI, which identifies a range of parameter values that, conditional on the observed data and prior information, contains the true parameter with a specified

posterior probability. The second is the HPD interval, defined as the shortest interval capturing the designated posterior probability mass, thus including only the most plausible values under the posterior distribution. The stepwise procedure for constructing both types of intervals is summarized in Algorithm 2.

Algorithm 2 Computation of BCI and HPD bounds for α and μ

1: **Input:** Posterior samples $\alpha^{(i)}$ and $\mu^{(i)}$ for $i = \mathbb{X}^{\bullet} + 1, \mathbb{X}^{\bullet} + 2, \ldots, \mathbb{X}$
2: **Output:** The $(1 - v)100\%$ BCI and HPD intervals for α and μ
3: **BCI/HPD bounds for α:**
4: Sort $\{\alpha^{(\mathbb{X}^{\bullet}+1)}, \ldots, \alpha^{(\mathbb{X})}\}$ such that $\alpha^{[1]} \leq \cdots \leq \alpha^{\bar{\mathbb{X}}}$
5: Compute BCI: $\left\{\alpha^{[0.5v\bar{\mathbb{X}}]},\ \alpha^{[(1-0.5v)\bar{\mathbb{X}}]}\right\}$
6: Compute HPD: $\left\{\alpha^{[i^{\star}]},\ \alpha^{[i^{\star}+((1-v)\bar{\mathbb{X}})]}\right\}$
7: where $i^{\star}$ is determined by
8:
$$\left\{\alpha^{[i^{\star}]},\ \alpha^{[i^{\star}+(1-v)\bar{\mathbb{X}}]}\right\} = \min_{1\leqslant i\leqslant v\bar{\mathbb{X}}}\left[\alpha^{[i+(1-v)\bar{\mathbb{X}}]} - \alpha^{[i]}\right].$$

9: **Repeat Steps 1–8** for μ

6. Simulation comparisons

In this section, we perform an extensive Monte Carlo simulation to examine how effectively the proposed estimators recover the DPham($\boldsymbol{\beta}$) parameters when applied to datasets generated under complete and incomplete sampling conditions.

6.1. Simulation design

To examine the behavior of the proposed methods considered for the DPham($\boldsymbol{\theta}$) distribution, we employ the generation design presented in Algorithm 3. All estimation results are assessed based on their average point estimate (APE), mean squared error (MSE), variance (Var), mean absolute bias (MAB), average interval length (AIL), and coverage percentage (CP).

Before proceeding, it is important to note that the parameter μ is restricted to the interval $(1, \infty)$ to ensure the validity of the proposed model. For the LF-based estimation, we adopt the transformation $\mu = 1 + \exp(\eta)$, where $\eta \in \mathbb{R}$, and perform the NR iterations on the transformed parameter η. This guarantees that all updated values automatically satisfy $\mu > 1$.

To enhance numerical stability and ensure reliable convergence, a step-size control mechanism (e.g., damped NR updates) is implemented. The iterative procedure is terminated when both the parameter change and the log-LF increase meet the convergence criteria

$$|\eta^{(t+1)} - \eta^{(t)}| < \epsilon \quad \text{and} \quad \left|\ell^{(t+1)} - \ell^{(t)}\right| < \epsilon,$$

for a prespecified tolerance $\epsilon > 0$. In the Bayesian framework, the prior distribution of μ is specified with support on $(1, \infty)$ via a shifted construction, ensuring that all posterior samples generated through MCMC remain within the admissible parameter space. Consequently, these strategies collectively ensure that both classical and Bayesian estimation procedures yield valid, stable, and consistent inference within the required parameter domain.

Algorithm 3 Simulation design for DPham distribution

Step 1: Set true sets of $\boldsymbol{\theta}$:

- Set-1: $\boldsymbol{\theta} = (0.5, 1.2)$;
- Set-2: $\boldsymbol{\theta} = (1.2, 1.5)$

Step 2: Set sample sizes $n \in \{20, 50, 100, 150, 200\}$

Step 3: Set failure percentage (FP) as FP $\in \left(\frac{r}{n}\right) \times 100\% \rightarrow$ FP $= \{40\%, 80\%, 100\%\}$

Step 4: Set hyperparameter options (a, b, c, d) according to the approach proposed by Kundu [26]:

- Prior-1 (P1): (2.5, 5, 1, 5) for Set-1; (6, 5, 2.5, 5) for Set-2;
- Prior-2 (P2): (5, 10, 2, 10) for Set-1; (12, 10, 5, 10) for Set-2

Step 5: Set computation scenarios:

- Number of replications: $\mathcal{N}_{rep} = 5000$
- Number of Markov iterations: $\wp = 12{,}000$, burn-in $\wp^{\bullet} = 2000$, remaining $\wp^{\star} = 12{,}000$

Step 6: Main Simulation Loop:

```
for each parameter set θ in {0.5, 1.5} do
    for each sample size n do
        for each censoring percentage FP100% do
            for i = 1 to N_rep do
                Generate n random variates u_i ~ U(0, 1)
                Transform: x_i = F^{-1}(u_i; θ)
                Sort {x_i} in ascending order
                Apply Type-II right censoring
                if Likelihood then
                    Run NR iterative algorithm by 'maxLik' package
                end if
                if Bayesian then
                    Use prior (1 or 2) based on parameter set
                    Run MCMC with ℘ iterations by 'coda' package
                end if
                Store point/interval estimates
            end for
        end for
    end for
end for
```

Step 7: Compute point estimation metrics:

- $\text{APE}(\hat{\alpha}) = \frac{1}{\mathcal{N}_{rep}} \sum_{i=1}^{\mathcal{N}_{rep}} \hat{\alpha}^{[i]}$; $\text{MSE}(\hat{\alpha}) = \frac{1}{\mathcal{N}_{rep}} \sum_{i=1}^{\mathcal{N}_{rep}} (\hat{\alpha}^{[i]} - \alpha)^2$; $\text{Var}(\hat{\alpha}) = \frac{1}{\mathcal{N}_{rep}} \sum_{i=1}^{\mathcal{N}_{rep}} (\hat{\alpha}^{[i]} - \text{APE}(\hat{\alpha}))^2$; $\text{MAB}(\hat{\alpha}) = \frac{1}{\mathcal{N}_{rep}} \sum_{i=1}^{\mathcal{N}_{rep}} |\hat{\alpha}^{[i]} - \alpha|$.

Step 8: Compute interval estimation metrics at $v = 5\%$:

- $\text{AIL}^{95\%}(\alpha) = \frac{1}{\mathcal{N}_{rep}} \sum_{i=1}^{\mathcal{N}_{rep}} (U_{\hat{\alpha}^{[i]}} - L_{\hat{\alpha}^{[i]}})$; $\text{CP}^{95\%}(\alpha) = \frac{1}{\mathcal{N}_{rep}} \sum_{i=1}^{\mathcal{N}_{rep}} \mathbb{I}_{[L_{\hat{\alpha}^{[i]}}, U_{\hat{\alpha}^{[i]}}]}(\alpha)$.

Step 9: Redo Steps 3–8 for μ

To assess the robustness of the Bayesian estimation process against different prior choices, we performed a sensitivity analysis incorporating several alternative prior specifications. This evaluation is especially important in censored lifetime models, where the posterior outcomes can be strongly influenced by the amount of prior information. As an example, we considered 1,000 CT2 samples generated from Set-1 and examined the resulting posterior distributions of the parameters α and μ under four distinct prior schemes: (i) informative (Prior-1), (ii) overdispersed with $\alpha \sim$ Gamma(0.5, 1) and $\mu \sim$ Gamma(0.2, 1), (iii) weakly informative with $\alpha \sim$ Gamma(1, 2) and $\mu \sim$ Gamma(0.4, 2), and (iv) improper with $\alpha, \mu \sim$ Uniform(0.01, 10). As illustrated in Figure 8, the posterior means are largely consistent across these priors, indicating robust inference. Among the alternatives, informative priors produce the narrowest Bayesian credible intervals and the lowest posterior standard deviations, highlighting their superior contribution to estimation precision.

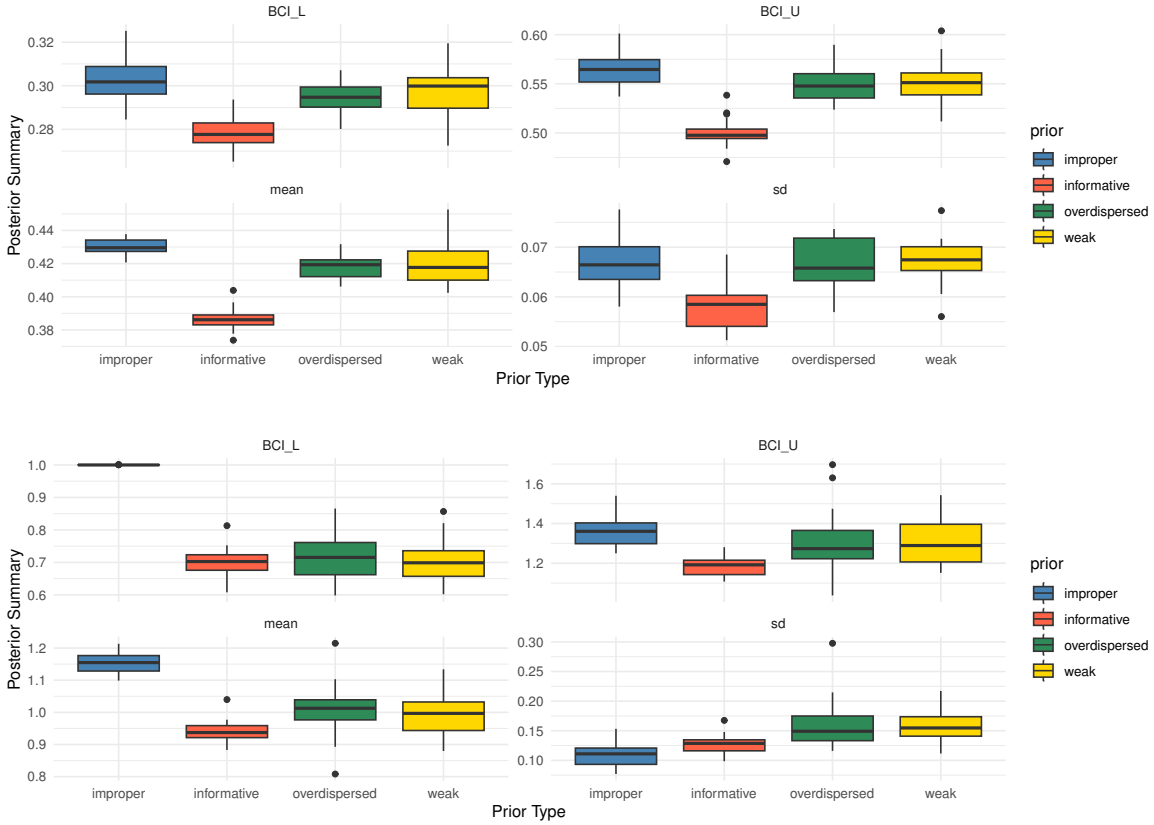

Figure 8. Sensitivity maps of α (top) and μ (bottom) using different priors from DPham(0.5,1.2).

6.2. *Simulation results*

Tables 3–6 summarize the Monte Carlo simulation outcomes obtained under various parameter configurations of the DPham($\boldsymbol{\theta}$) model. The key findings and methodological insights, derived from the lowest values of the MSE, MAB, and AIL, as well as the highest CP values, are presented as follows:

- The estimation accuracy of α and μ improves as n (or r) increases, confirming the consistency and robustness of the proposed estimators. Moreover, higher levels of FP% contribute to improved estimation precision across all methods.
- Bayesian estimators (MCMC-based) consistently outperform their frequentist counterparts, particularly for small samples, underscoring the advantage of incorporating prior information into the estimation process.
- Credible intervals derived from BCI and HPD methods demonstrate superior coverage performance compared with asymptotic approaches such as ACI[NA] and ACI[NL].
- Employing an informative gamma prior for the DPham parameters significantly enhances the accuracy of both Bayesian point and interval estimators relative to the frequentist methods.
- Efficiency improvements are achieved when using P2 in MCMC-based Bayesian estimation, as it produces lower variance compared to P1.
- Point estimation performance is consistently better for Set-1 than for its alternative configuration, indicating that smaller values of $\boldsymbol{\theta}$ yield more reliable and precise estimates.
- Comparing the estimation frameworks proposed, we noted the following:
  - For point estimation, the Bayesian framework consistently outperforms the likelihood-based framework across all settings.
  - For interval estimations:
    * HPD intervals provide the most satisfactory performance for both DPham parameters;
    * ACI[NA] performs better than ACI[NL] for α, whereas the opposite behavior is noted for μ;
    * The BCI and HPD intervals are generally more precise and reliable than both asymptotic intervals.
- As $\boldsymbol{\theta}$ increases, the following patterns are observed:
  - The MSE and MAB results of both maximum likelihood and Bayesian estimators for α or μ tend to increase;
  - The AIL values for all interval estimation methods increase for α and μ, whereas the associated CP values decrease.
- Overall, Bayesian inference, particularly when employing HPD or BCI intervals, demonstrates strong performance under both complete and censored data scenarios, yielding accurate and reliable estimates even in the presence of incomplete (censored) observations.

Figures 9 and 10 provide comprehensive graphical summaries of the simulation study, illustrating the behavior of key performance metrics, including MSE, Var, MAB, AIL, and CP, under various configurations of the DPham($\boldsymbol{\theta}$) parameters. The plots reveal clear trends in estimator performance that when n tends to be large or FP% of observed r units grows to be complete, the MSE, Var, and MAB generally decrease, whereas the CP remains stable, particularly for BCIs. Variations in AIL across different methods highlight the relative precision of interval estimates, with HPD and BCI intervals consistently showing narrower lengths compared to asymptotic intervals. These visualizations not only corroborate the numerical results presented in Tables 3–6 but also offer intuitive insights into the comparative efficiency and reliability of the proposed estimators across both complete and censored data scenarios.

Table 3. The APE (1^{st} col.), MSE (2^{nd} col.), Var (3^{rd} col.), and MAB (4^{th} col.) of α (1^{st} row) and μ (2^{nd} row) for Set-1.

n	FP%	MLE				Bayes[P1]				Bayes[P2]			
20	40%	0.5539	0.2419	0.1711	0.2218	0.6446	0.0771	0.0545	0.0591	0.6132	0.0516	0.0199	0.0233
		1.1981	0.0912	0.0667	0.0787	1.1679	0.0095	0.0068	0.0073	1.1752	0.0068	0.0043	0.0049
	80%	0.5390	0.2409	0.1240	0.1824	0.5430	0.0688	0.0254	0.0461	0.5413	0.0253	0.0150	0.0215
		1.1949	0.0813	0.0602	0.0765	1.1921	0.0073	0.0057	0.0066	1.1920	0.0057	0.0036	0.0040
	100%	0.5337	0.1683	0.0920	0.1445	0.4670	0.0442	0.0149	0.0327	0.4702	0.0133	0.0101	0.0105
		1.1931	0.0612	0.0563	0.0602	1.2252	0.0056	0.0049	0.0049	1.2208	0.0049	0.0032	0.0036
50	40%	0.5100	0.0890	0.0867	0.0885	0.7358	0.0115	0.0109	0.0112	0.6762	0.0103	0.0080	0.0087
		1.2037	0.0597	0.0521	0.0581	1.1097	0.0049	0.0043	0.0047	1.1229	0.0043	0.0025	0.0028
	80%	0.5196	0.0874	0.0747	0.0821	0.5443	0.0106	0.0096	0.0098	0.5468	0.0084	0.0054	0.0059
		1.1998	0.0562	0.0472	0.0547	1.1428	0.0047	0.0036	0.0043	1.1407	0.0036	0.0022	0.0025
	100%	0.5164	0.0869	0.0692	0.0811	0.5416	0.0104	0.0080	0.0097	0.5483	0.0076	0.0047	0.0054
		1.1986	0.0548	0.0441	0.0519	1.1475	0.0042	0.0031	0.0039	1.1433	0.0031	0.0017	0.0020
100	40%	0.4832	0.0826	0.0691	0.0782	0.7415	0.0099	0.0075	0.0086	0.7213	0.0069	0.0044	0.0049
		1.2045	0.0538	0.0380	0.0510	1.1188	0.0040	0.0023	0.0037	1.1236	0.0023	0.0014	0.0018
	80%	0.5070	0.0741	0.0642	0.0715	0.5840	0.0089	0.0061	0.0081	0.5780	0.0053	0.0037	0.0040
		1.2009	0.0524	0.0344	0.0496	1.1508	0.0036	0.0019	0.0033	1.1537	0.0019	0.0013	0.0017
	100%	0.5079	0.0666	0.0545	0.0645	0.5860	0.0074	0.0048	0.0069	0.5797	0.0045	0.0036	0.0038
		1.1993	0.0515	0.0313	0.0493	1.1476	0.0035	0.0016	0.0032	1.1510	0.0016	0.0012	0.0015
150	40%	0.4757	0.0641	0.0478	0.0604	0.5546	0.0060	0.0037	0.0060	0.5523	0.0036	0.0035	0.0036
		1.2051	0.0480	0.0312	0.0472	1.1534	0.0030	0.0015	0.0029	1.1542	0.0015	0.0011	0.0014
	80%	0.5031	0.0602	0.0386	0.0589	0.5524	0.0053	0.0026	0.0053	0.5517	0.0024	0.0024	0.0024
		1.2017	0.0439	0.0283	0.0437	1.1583	0.0025	0.0013	0.0025	1.1586	0.0013	0.0010	0.0012
	100%	0.5036	0.0577	0.0375	0.0559	0.5238	0.0052	0.0025	0.0051	0.5222	0.0023	0.0022	0.0023
		1.2007	0.0355	0.0271	0.0341	1.1687	0.0018	0.0012	0.0016	1.1695	0.0011	0.0008	0.0011
200	40%	0.4719	0.0358	0.0333	0.0335	0.4198	0.0020	0.0018	0.0018	0.4183	0.0018	0.0015	0.0015
		1.2051	0.0265	0.0257	0.0259	1.2030	0.0015	0.0011	0.0013	1.2035	0.0010	0.0007	0.0010
	80%	0.5014	0.0312	0.0300	0.0309	0.4977	0.0015	0.0015	0.0015	0.4995	0.0014	0.0013	0.0014
		1.2016	0.0256	0.0246	0.0255	1.1896	0.0013	0.0011	0.0012	1.1884	0.0009	0.0007	0.0009
	100%	0.5025	0.0300	0.0256	0.0297	0.5192	0.0014	0.0010	0.0014	0.5185	0.0010	0.0010	0.0010
		1.2005	0.0242	0.0221	0.0236	1.1817	0.0012	0.0010	0.0011	1.1821	0.0008	0.0006	0.0008

Table 4. The APE (1^{st} col.), MSE (2^{nd} col.), Var (3^{rd} col.), and MAB (4^{th} col.) of α (1^{st} row) and μ (2^{nd} row) for Set-1.

n	FP%	MLE				Bayes[P1]				Bayes[P2]			
20	40%	0.7935	1.2199	1.0994	1.1535	0.8787	1.0700	0.7019	0.8325	1.8868	0.1111	0.0416	0.1029
		1.4455	0.2333	0.1201	0.2149	0.4852	0.0579	0.0207	0.0501	1.4991	0.0196	0.0194	0.0195
	80%	1.0190	1.1059	0.9149	1.0459	1.0335	0.8458	0.5133	0.6890	1.4887	0.0790	0.0358	0.0476
		1.5230	0.1611	0.1123	0.1401	0.5801	0.0285	0.0194	0.0233	1.4172	0.0180	0.0066	0.0074
	100%	1.3112	1.0352	0.7836	1.0080	1.1211	0.6682	0.4668	0.6392	1.2268	0.0773	0.0214	0.0253
		1.4874	0.1583	0.1051	0.1385	0.5440	0.0285	0.0185	0.0227	1.4345	0.0121	0.0052	0.0057
50	40%	0.7412	0.9231	0.7563	0.8882	0.5635	0.6677	0.4600	0.5862	0.8677	0.0672	0.0203	0.0232
		1.4612	0.1451	0.0890	0.1377	0.3947	0.0250	0.0121	0.0224	1.2667	0.0111	0.0046	0.0051
	80%	0.9955	0.8166	0.4547	0.7305	0.7876	0.3473	0.1462	0.2408	1.0917	0.0597	0.0197	0.0206
		1.5312	0.1336	0.0877	0.1307	0.4542	0.0214	0.0121	0.0210	1.3571	0.0061	0.0043	0.0049
	100%	1.2542	0.4131	0.3201	0.3363	0.7640	0.1917	0.1188	0.1356	1.2823	0.0540	0.0162	0.0178
		1.4979	0.1236	0.0851	0.1167	0.4260	0.0207	0.0114	0.0195	1.3688	0.0055	0.0042	0.0046
100	40%	0.6678	0.3484	0.2933	0.3122	0.3253	0.1343	0.1048	0.1275	0.5318	0.0504	0.0158	0.0175
		1.4725	0.1201	0.0655	0.1117	0.2905	0.0191	0.0069	0.0158	1.3419	0.0050	0.0035	0.0042
	80%	0.9462	0.3111	0.2922	0.3093	0.5276	0.1286	0.0953	0.1063	0.9079	0.0397	0.0145	0.0169
		1.5369	0.1021	0.0628	0.0969	0.3221	0.0131	0.0061	0.0126	1.4644	0.0040	0.0034	0.0040
	100%	1.2264	0.3057	0.2697	0.2786	0.5218	0.1241	0.0807	0.0861	1.4106	0.0362	0.0142	0.0142
		1.4985	0.1001	0.0615	0.0941	0.3006	0.0123	0.0060	0.0117	1.4096	0.0037	0.0031	0.0033
150	40%	0.6415	0.3002	0.2146	0.2350	0.2359	0.1207	0.0589	0.0703	0.5323	0.0193	0.0100	0.0107
		1.4789	0.0944	0.0586	0.0937	0.2415	0.0120	0.0054	0.0113	1.3389	0.0035	0.0030	0.0032
	80%	0.9267	0.2234	0.1998	0.2162	0.4219	0.0895	0.0482	0.0555	0.9304	0.0182	0.0089	0.0104
		1.5411	0.0943	0.0546	0.0920	0.2639	0.0111	0.0046	0.0109	1.4483	0.0030	0.0026	0.0028
	100%	1.2138	0.1615	0.1448	0.1592	0.4204	0.0426	0.0314	0.0372	1.3146	0.0120	0.0088	0.0090
		1.5007	0.0935	0.0503	0.0881	0.2460	0.0106	0.0040	0.0094	1.4069	0.0028	0.0025	0.0028
200	40%	0.5933	0.1373	0.1086	0.1238	0.1865	0.0270	0.0189	0.0226	0.3675	0.0116	0.0084	0.0087
		1.4818	0.0623	0.0490	0.0618	0.2116	0.0069	0.0039	0.0054	1.3840	0.0025	0.0022	0.0024
	80%	0.9102	0.1271	0.0849	0.1209	0.3582	0.0257	0.0117	0.0220	0.8637	0.0087	0.0081	0.0085
		1.5429	0.0610	0.0437	0.0597	0.2287	0.0056	0.0030	0.0053	1.4823	0.0023	0.0015	0.0022
	100%	1.2107	0.1131	0.0735	0.1060	0.3625	0.0193	0.0087	0.0169	1.3993	0.0086	0.0058	0.0062
		1.4999	0.0469	0.0410	0.0430	0.2127	0.0029	0.0028	0.0029	1.4125	0.0018	0.0012	0.0018

Table 5. The AIL (1^{st} col.) and CPs (2^{nd} col.) of α (1^{st} row) and μ (2^{nd} row) for Set-1.

n	FP%	ACI[NA]		ACI[NL]		BCI[P1]		BCI[P2]		HPD[P1]		HPD[P2]	
20	40%	0.953	0.942	0.965	0.941	0.909	0.944	0.822	0.949	0.497	0.967	0.475	0.968
		0.955	0.932	0.950	0.932	0.323	0.968	0.322	0.968	0.245	0.972	0.241	0.973
	80%	0.950	0.942	0.958	0.941	0.630	0.960	0.593	0.962	0.465	0.969	0.448	0.970
		0.952	0.932	0.949	0.932	0.294	0.970	0.293	0.970	0.226	0.974	0.222	0.974
	100%	0.947	0.942	0.953	0.942	0.461	0.969	0.448	0.970	0.402	0.972	0.389	0.973
		0.948	0.932	0.947	0.932	0.270	0.971	0.270	0.971	0.218	0.974	0.211	0.974
50	40%	0.945	0.942	0.953	0.942	0.410	0.972	0.398	0.972	0.348	0.975	0.335	0.976
		0.946	0.933	0.946	0.933	0.256	0.972	0.256	0.972	0.158	0.977	0.144	0.978
	80%	0.914	0.944	0.952	0.942	0.355	0.975	0.349	0.975	0.274	0.979	0.272	0.980
		0.942	0.933	0.940	0.933	0.232	0.973	0.232	0.973	0.143	0.978	0.140	0.978
	100%	0.863	0.947	0.951	0.942	0.342	0.976	0.336	0.976	0.263	0.980	0.252	0.981
		0.940	0.933	0.938	0.933	0.213	0.974	0.213	0.974	0.140	0.978	0.134	0.979
100	40%	0.682	0.957	0.948	0.942	0.327	0.976	0.321	0.977	0.252	0.981	0.244	0.981
		0.937	0.933	0.937	0.933	0.182	0.976	0.182	0.976	0.129	0.979	0.126	0.979
	80%	0.526	0.965	0.947	0.942	0.280	0.979	0.276	0.979	0.244	0.981	0.233	0.982
		0.933	0.933	0.929	0.933	0.165	0.977	0.165	0.977	0.124	0.979	0.122	0.979
	100%	0.450	0.970	0.921	0.943	0.263	0.980	0.260	0.980	0.241	0.981	0.230	0.982
		0.927	0.934	0.926	0.934	0.151	0.978	0.151	0.978	0.115	0.980	0.113	0.980
150	40%	0.423	0.971	0.891	0.945	0.235	0.982	0.235	0.982	0.234	0.982	0.222	0.982
		0.924	0.934	0.923	0.934	0.149	0.978	0.149	0.978	0.111	0.980	0.106	0.980
	80%	0.387	0.973	0.852	0.947	0.196	0.984	0.196	0.984	0.195	0.984	0.190	0.984
		0.920	0.934	0.917	0.934	0.136	0.979	0.135	0.979	0.109	0.980	0.104	0.980
	100%	0.370	0.974	0.760	0.952	0.186	0.984	0.186	0.984	0.185	0.984	0.168	0.985
		0.920	0.934	0.915	0.934	0.129	0.979	0.129	0.979	0.108	0.980	0.103	0.981
200	40%	0.364	0.974	0.444	0.970	0.163	0.986	0.162	0.986	0.160	0.986	0.153	0.986
		0.919	0.934	0.913	0.934	0.124	0.979	0.124	0.979	0.105	0.980	0.101	0.981
	80%	0.352	0.975	0.417	0.971	0.146	0.987	0.145	0.987	0.144	0.987	0.138	0.987
		0.910	0.935	0.905	0.935	0.117	0.980	0.117	0.980	0.104	0.980	0.099	0.981
	100%	0.297	0.978	0.343	0.976	0.126	0.988	0.126	0.988	0.125	0.988	0.119	0.988
		0.907	0.935	0.900	0.935	0.107	0.980	0.107	0.980	0.097	0.981	0.095	0.981

Table 6. The AIL (1^{st} col.) and CP (2^{nd} col.) of α (1^{st} row) and μ (2^{nd} row) for Set-2.

n	FP%	ACI[NA]		ACI[NL]		BCI[P1]		BCI[P2]		HPD[P1]		HPD[P2]	
20	40%	1.299	0.945	1.509	0.937	1.000	0.956	0.948	0.958	0.767	0.964	0.732	0.966
		1.123	0.929	0.970	0.937	0.622	0.954	0.584	0.956	0.515	0.960	0.492	0.961
	80%	1.156	0.950	1.486	0.938	0.979	0.957	0.945	0.958	0.714	0.966	0.682	0.967
		1.117	0.929	0.968	0.937	0.583	0.956	0.547	0.958	0.359	0.968	0.343	0.968
	100%	1.080	0.953	1.436	0.940	0.968	0.957	0.944	0.958	0.554	0.972	0.529	0.973
		1.104	0.930	0.964	0.937	0.519	0.960	0.488	0.961	0.296	0.971	0.283	0.972
50	40%	1.228	0.950	1.416	0.940	0.944	0.958	0.809	0.963	0.550	0.972	0.526	0.973
		1.090	0.931	0.954	0.938	0.486	0.961	0.456	0.963	0.259	0.972	0.247	0.973
	80%	1.117	0.953	1.329	0.944	0.935	0.958	0.776	0.964	0.499	0.974	0.477	0.975
		1.070	0.932	0.946	0.938	0.455	0.963	0.427	0.964	0.253	0.973	0.241	0.974
	100%	0.977	0.958	1.291	0.945	0.737	0.965	0.711	0.966	0.482	0.975	0.460	0.976
		1.056	0.932	0.944	0.938	0.422	0.964	0.396	0.966	0.248	0.973	0.237	0.974
100	40%	1.126	0.952	1.238	0.947	0.603	0.970	0.535	0.973	0.467	0.975	0.446	0.976
		1.055	0.932	0.944	0.938	0.344	0.968	0.323	0.969	0.231	0.974	0.221	0.975
	80%	0.975	0.955	1.171	0.949	0.466	0.975	0.466	0.975	0.446	0.976	0.426	0.977
		1.051	0.933	0.937	0.938	0.321	0.970	0.301	0.971	0.227	0.974	0.217	0.975
	100%	0.945	0.958	0.945	0.958	0.450	0.976	0.442	0.976	0.442	0.976	0.414	0.978
		1.045	0.933	0.934	0.939	0.310	0.970	0.291	0.971	0.215	0.975	0.205	0.975
150	40%	1.095	0.956	0.944	0.958	0.386	0.978	0.386	0.978	0.384	0.978	0.366	0.979
		1.036	0.933	0.925	0.939	0.281	0.972	0.264	0.972	0.213	0.975	0.204	0.976
	80%	0.921	0.957	0.903	0.959	0.379	0.979	0.379	0.979	0.374	0.979	0.358	0.979
		1.029	0.934	0.924	0.939	0.262	0.973	0.246	0.973	0.198	0.976	0.189	0.976
	100%	0.910	0.958	0.808	0.963	0.370	0.979	0.364	0.979	0.350	0.980	0.334	0.980
		1.024	0.934	0.924	0.939	0.258	0.973	0.242	0.974	0.196	0.976	0.188	0.976
200	40%	0.916	0.959	0.474	0.975	0.364	0.979	0.360	0.979	0.348	0.980	0.333	0.981
		1.023	0.934	0.920	0.939	0.244	0.973	0.229	0.974	0.195	0.976	0.186	0.976
	80%	0.911	0.959	0.447	0.976	0.352	0.980	0.336	0.981	0.336	0.981	0.261	0.983
		1.020	0.934	0.919	0.939	0.227	0.974	0.213	0.975	0.182	0.977	0.174	0.977
	100%	0.901	0.960	0.320	0.981	0.295	0.982	0.295	0.982	0.285	0.982	0.203	0.985
		0.964	0.937	0.880	0.941	0.226	0.974	0.212	0.975	0.162	0.978	0.155	0.978

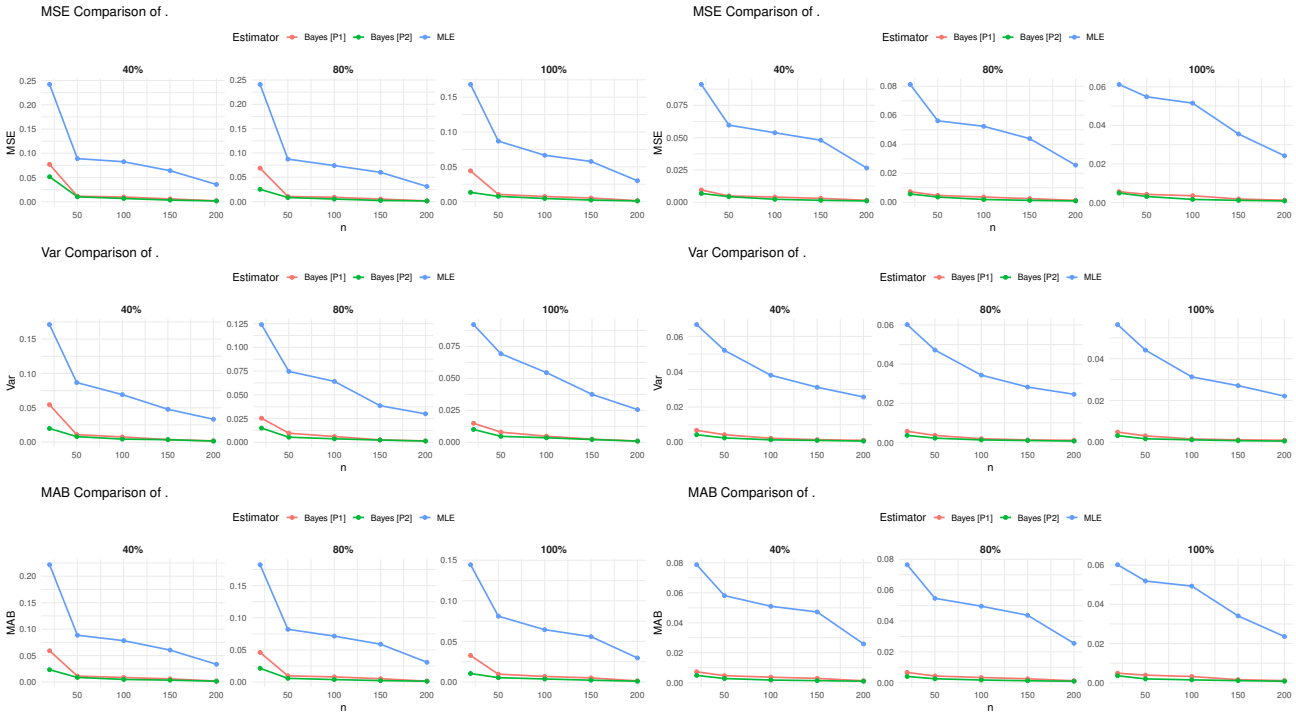

(a) For Set-1

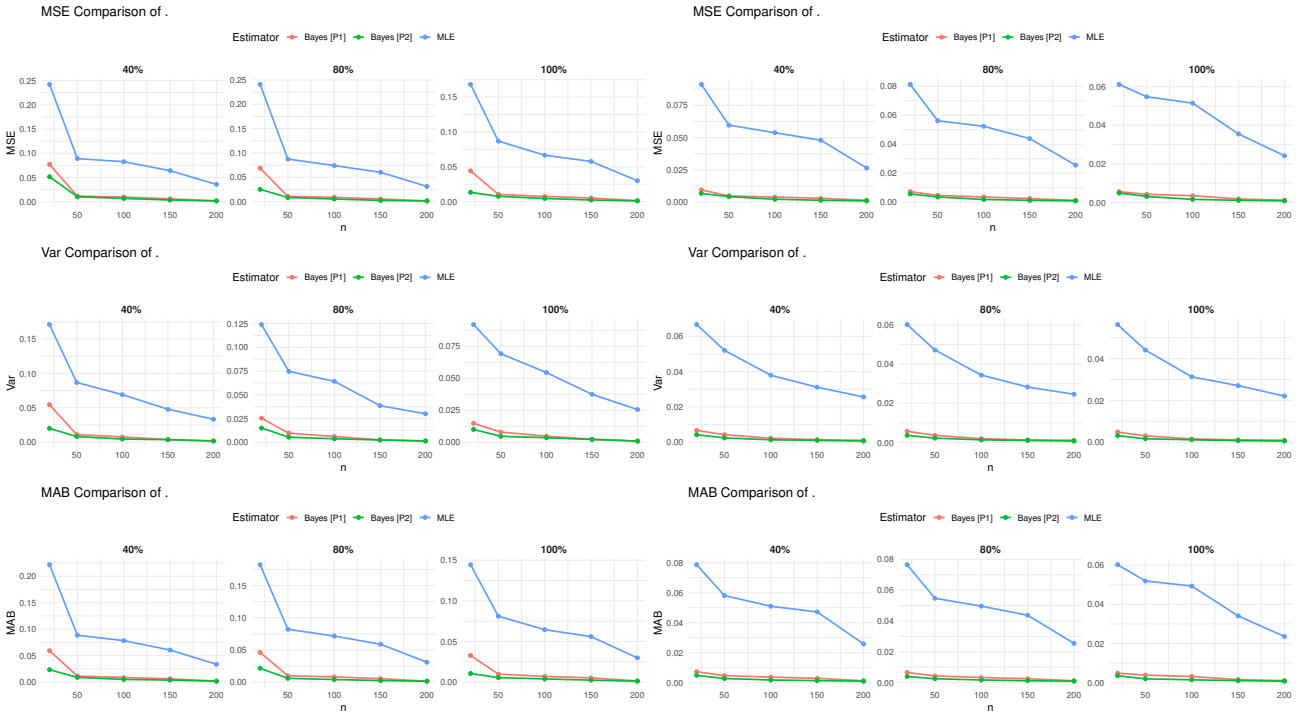

(b) For Set-2

Figure 9. Plot of the MSE (left), Var (center), and MAB (right) results of α and μ.

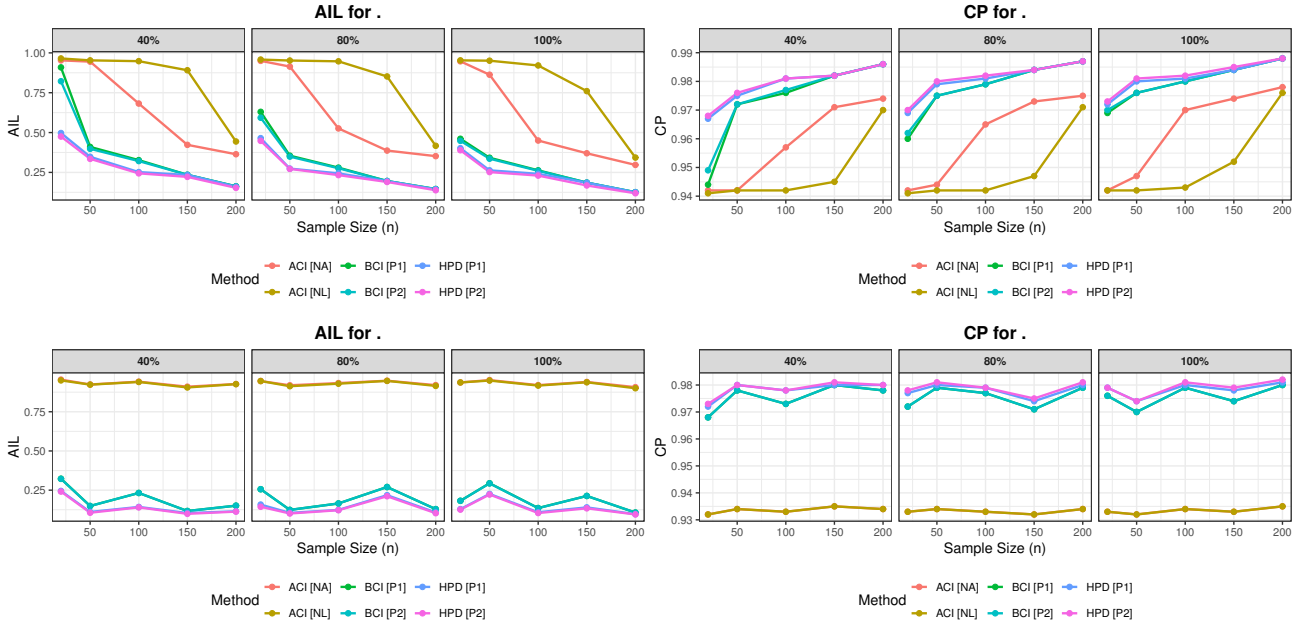

(a) For Set-1

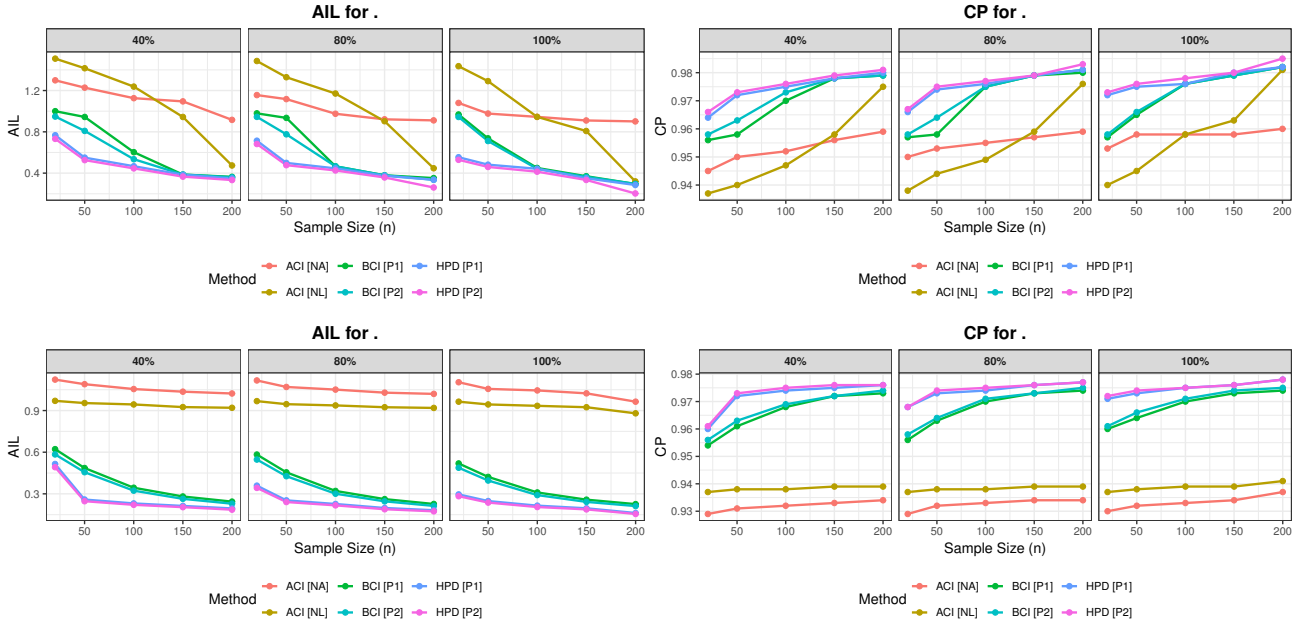

(b) For Set-2

Figure 10. Plot of the AIL (left) and CP (right) results of α and μ.

7. Real data applications

This section investigates three distinct real-world datasets that represent valuable case studies for modeling discrete lifetime data. These datasets originate from clinical, engineering, and physical domains, thereby encompassing a diverse range of practical applications. The objectives of this analysis are threefold: (i) to evaluate the flexibility, effectiveness, and practical relevance of the proposed DPham model; (ii) to demonstrate the applicability and interpretive value of the model's

inferential results in real-world decision-making contexts; and (iii) to benchmark its goodness-of-fit and inferential performance against eleven well-established discrete lifetime distributions. Table 7 provides an overview of the datasets used in this comparative study, including their origins, sample sizes, and key characteristics, as follows:

- **Application 1:** The analysis of remission duration among leukemia patients following treatment plays a crucial role in evaluating therapeutic efficacy. In this application, remission times (measured in weeks) were recorded for a cohort of 20 leukemia patients who were randomly assigned to a specific treatment protocol. This dataset (Data-1) was originally introduced by Bakouch et al. [27] and reanalyzed by Eliwa and El-Morshedy [28].
- **Application 2:** This application addresses reliability analysis in industrial engineering, focusing on the failure times (in hours) of 18 electronic devices. This dataset (Data-2) was originally introduced by Wang [29] and has since been widely employed to assess the suitability of lifetime distributions for modeling empirical reliability data; see, for example, Elshahhat and Abu El Azm [30].
- **Application 3:** This application considers a dataset comprising 20 observations representing the number of shocks sustained before system failure. This dataset (Data-3) provides a practical basis for modeling and analyzing the reliability behavior of units operating under random shock environments; see Murthy et al. [31] and Cordeiro et al. [32].

Table 7. Three datasets from clinical, engineering, and physical sectors.

Data-1									
1	3	3	6	7	7	10	12	14	15
18	19	22	26	28	29	34	40	48	49
Data-2									
5	11	21	31	46	75	98	122	145	165
196	224	245	293	321	330	350	420		
Data-3									
2	3	6	6	7	9	9	10	10	11
12	12	12	13	13	13	15	16	16	18

It is noteworthy that the three datasets analyzed in this study provide a diverse empirical foundation, highlighting the adaptability of the proposed model across different application domains. Each dataset exhibits complex real-world features, including discreteness and deviations from normality, which introduce additional challenges in both model fitting and validation.

Table 8 presents the descriptive statistics for each dataset (Data-i, $i = 1, 2, 3$), reporting the range (minimum and maximum), quartiles (Q_i, $i = 1, 2, 3$), measures of central tendency (mean and mode), standard deviation (SD), and distributional shape characteristics (skewness and kurtosis). The findings reveal that Data-i for $i = 1, 2$ display greater dispersion and noticeable right skewness, whereas Data-3 exhibits mild left skewness. All datasets show mesokurtic behavior (kurtosis < 3), indicating moderate tail thickness and near-normal peakedness.

Table 8. Statistical summary for three real datasets.

Data	Min	Max	Q_1	Q_2	Q_3	Mode	Mean	SD	Skew.	Kurt.
Data-1	1	49	7	16.5	28.25	3	19.550	14.70	0.653	2.380
Data-2	5	420	53.25	155	281	5	172.11	131.5	0.314	1.850
Data-3	2	18	8.5	11.5	13	12	10.650	4.283	-0.359	2.497

A violin plot combines the advantages of a traditional boxplot with kernel density estimation, providing an integrated view of both key summary statistics and the underlying probability structure of a given dataset. Figure 11 displays violin plots for the three datasets (Data-i, $i = 1, 2, 3$), providing a comprehensive visualization of their distributional characteristics. The estimated total time on test (TTT) transform is one of the most informative graphical tools in reliability analysis, which allows one to visually reveal the shape of the risk rate in the data or any distribution; see Figure 11.

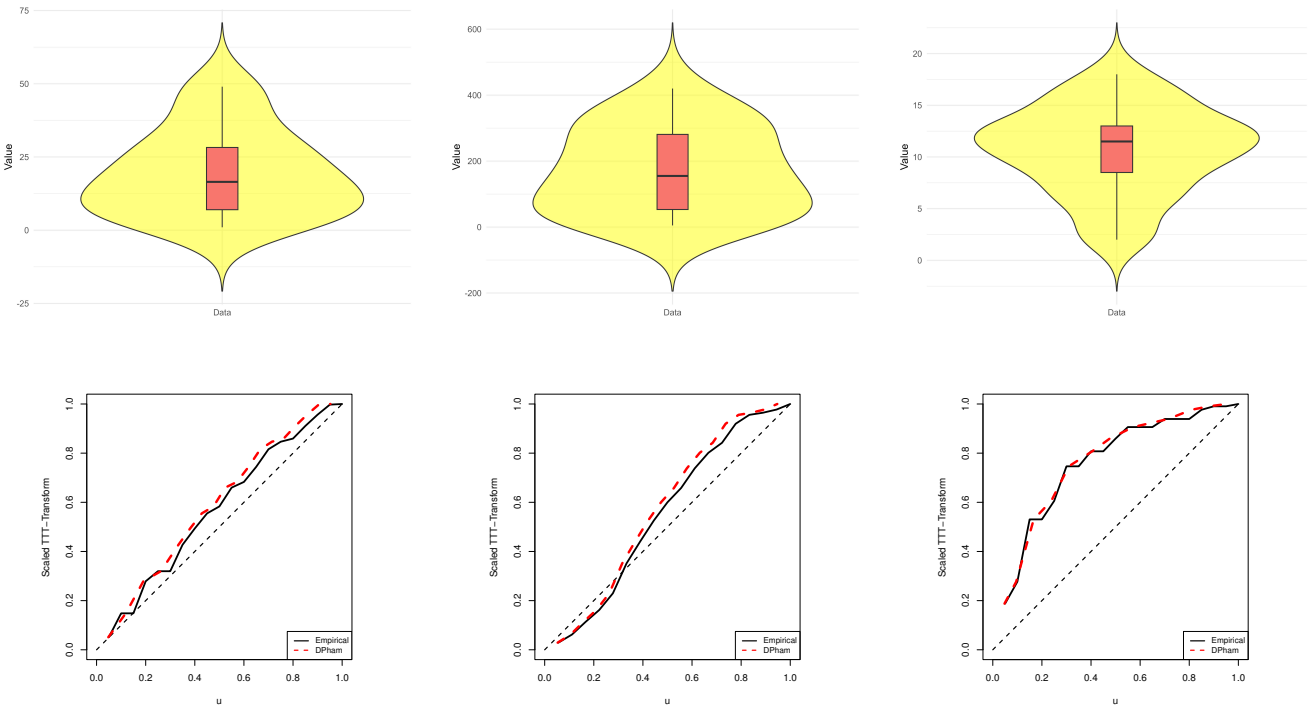

(a) Data-1 (b) Data-2 (c) Data-3

Figure 11. Violin (top) and TTT (bottom) diagrams of the DPham distribution from three real datasets.

As a sequence, we noted the following

- Figure 11(a) shows
  - Data-1 displays moderately right-skewed, with most observations concentrated between approximately 5 and 25. The relatively narrow spread indicates consistent measurements, with only a few higher values extending the upper tail;

  - Data-2 exhibits substantial variability and a pronounced right skew. The median lies near the lower quartile, suggesting that while most values are small, several large outliers stretch the upper tail, increasing overall dispersion;
  - Data-3 follows a compact and slightly left-skewed distribution, with most observations clustering around 10 to 12. The limited spread implies low measurement variability and potentially a stable underlying process,

- Figure 11(b) shows
  - Data-i, $i = 1, 3$ exhibit increasing failure rates;
  - Data-2 produces a bathtub-shaped failure rate;
  - All failure rate patterns associated with Data-i, $i = 1, 2, 3$, are consistent with the theoretical DPham hazard rates shown in Figure 1.

Now, to further illustrate the adaptability, flexibility, and effectiveness of the proposed DPham distribution, a comprehensive comparative analysis is conducted. Using the datasets summarized in Table 7, the fit performance of the DPham model is systematically evaluated against nine benchmark discrete distributions commonly employed in the literature, namely:

(1) Geometric, Geom(μ), Johnson et al. [33];
(2) Negative binomial, NB(α, μ), Johnson et al. [33];
(3) Discrete Nadarajah-Haghighi, DNH(α, μ), Shafqat et al. [34];
(4) Discrete Perks, DP(α, μ), Tyagi et al. [35];
(5) Discrete Weibull, DW(α, μ), Nakagawa and Osaki [36];
(6) Discrete gamma, DG(α, μ), Chakraborty and Chakravarty [37];
(7) Discrete exponentiated-Chen, DEC(β, α, μ), Alotaibi et al. [38];
(8) Exponentiated discrete Weibull, EDW(β, α, μ), Nekoukhou and Bidram [39];
(9) Discrete modified Weibull, DMW(β, α, μ), Almalki and Nadarajah [40].

This comparative framework enables a rigorous assessment of the proposed model's empirical adequacy and its relative superiority in modeling diverse forms of discrete lifetime data. To identify the most suitable model among the proposed DPham distribution and its competing alternatives, a comprehensive model comparison was performed using a suite of model selection and goodness-of-fit criteria. These include the negative log-likelihood (NLL), Akaike information (AI), consistent AI (CAI), Bayesian information (BI), and Hannan-Quinn information (HQI), in addition to the Kolmogorov-Smirnov (KS) statistic and its associated $\mathcal{P}$-value. Table 9 presents the MLEs of β, α, and μ along with their corresponding standard errors (SEs), for all datasets. It also reports the computed values of all selection and fit criteria for the competing distributions proposed. The results in Table 9 clearly demonstrate that the proposed DPham distribution consistently attains the lowest values for all information-based metrics, indicating a superior overall fit. Moreover, it achieves the smallest KS statistic and the highest corresponding $\mathcal{P}$-value among all candidate models. Collectively, these findings in Table 9 confirm that the DPham distribution provides the best empirical fit and is, therefore, the most appropriate model for analyzing the considered datasets.

Graphical goodness-of-fit assessments provide essential insights into how well a theoretical model represents observed data. Figure 12 highlights the effectiveness of the DPham model through multiple visualization techniques: (i) fitted PMF curves superimposed on empirical histograms, (ii) plots of the

fitted survival (reliability) functions, (iii) probability-probability (PP) plots, and (iv) quantile-quantile (QQ) plots. These visual diagnostics, together with the numerical results presented in Figure 12 and Table 9, clearly indicate that the DPham distribution provides a consistently superior fit relative to other traditional and modern discrete lifetime models across all examined datasets.

To evaluate the performance of the estimators for the DPham($\boldsymbol{\theta}$) parameters obtained via maximum likelihood and Bayesian inference (using $\wp = 40{,}000$ and $\wp^{\bullet} = 10{,}000$ iterations), three failure censored samples, corresponding to different censoring levels r, were generated from each dataset listed in Table 7. For every censored sample, point estimates (with their associated SEs) and 95% interval estimates (together with interval widths) for α and μ were computed, and the results are reported in Table 10. A comparison of these results shows that the Bayesian point estimators consistently achieve smaller SEs than their frequentist (likelihood-based) counterparts, indicating superior estimation precision within the Bayesian framework. Moreover, the credible interval methods (BCI and HPD) yield noticeably narrower interval widths than the frequentist asymptotic intervals (ACI[NA] and ACI[NL]), further demonstrating the efficiency of Bayesian interval estimation. As expected, increases in the number of observed units r lead to decreases in both SEs and interval widths for the estimates of α and μ, reflecting improved efficiency as censoring is reduced. To examine the existence and uniqueness of $\hat{\alpha}$ and $\hat{\mu}$, and to gain insights into the stability and sensitivity of the DPham estimators of α and μ, contour plots of the log-likelihood function were constructed, as shown in Figure 13(a). These contour diagrams illustrate how the log-likelihood varies jointly with α and μ, providing a visual assessment of the likelihood surface. The subplots in Figure 13 correspond to the representative cases $(n, r) = (20, 8)$, $(18, 8)$, and $(20, 60)$ for Data-i, $i = 1, 2, 3$, respectively. As a result, Figure 13 confirms that the fitted estimates $\hat{\alpha}$ and $\hat{\mu}$ exist and are unique for all datasets. These results reinforce the accuracy and reliability of the estimates reported in Table 10, thereby supporting the validity of the proposed model. Based on these findings, we recommend using the corresponding frequency-based estimates as initial values for the Markov chain iterations to ensure stable and efficient convergence during the Bayesian estimation process.

An essential aspect of the Bayesian analysis is verifying adequate convergence of the MCMC algorithm. Figure 13(b) displays the trace plots and posterior density estimates for α and μ, where each panel includes the posterior mean (solid) and the corresponding 95% BCI bounds (dashed). These graphical diagnostics indicate that the proposed M-H algorithm attains stable convergence, and the resulting posterior distributions for all datasets (Data-i, $i = 1, 2, 3$) are approximately symmetric. Complementing these visual assessments, Table 11 provides detailed posterior summaries for α and μ based on 30,000 retained MCMC samples. These numerical findings closely align with the results in Table 10 and reinforce the graphical evidence shown in Figure 13(b). Together, they confirm the robustness and reliability of the Bayesian inference procedures employed for the DPham distribution.

Overall, the analysis of all datasets (Data-i, $i = 1, 2$) demonstrates that the proposed DPham distribution possesses strong statistical properties, exhibiting robust performance, high flexibility, and superior empirical fit when compared with both classical and modern discrete models. Its adaptability across diverse application domains, together with its reliable inferential behavior, particularly within the Bayesian framework, underscores its value as a practically useful and theoretically sound model for discrete data analysis. These findings highlight the importance of newly developed discrete distributions in capturing complex real-world data structures and illustrate their potential to advance model evaluation and parameter estimation across a range of scientific disciplines.

Table 9. Fitting outcomes of the DPham and its competitors from three real datasets.

Model	β		α		μ		NLL	AI	CAI	BI	HQI	KS	
	Est.	SE	Est.	SE	Est.	SE						Distance	$\mathcal{P}$-value
Data-1													
DPham	-	-	1.0360	0.1993	1.0264	0.0198	78.407	160.813	161.519	162.805	161.202	0.0772	0.9998
Geom	-	-	-	-	0.0487	0.0106	79.963	161.925	162.147	162.921	162.119	0.1447	0.7961
NB	-	-	1.6865	0.5617	19.551	3.5088	78.812	161.623	162.329	163.615	162.012	0.0934	0.9949
DNH	-	-	5.6596	5.3227	0.0058	0.0060	78.521	161.042	161.748	163.033	161.430	0.0776	0.9997
DP	-	-	0.0842	0.0261	0.4437	0.4747	78.814	161.628	162.334	163.619	162.016	0.0782	0.9997
DW	-	-	1.3741	0.2478	21.912	3.7548	78.612	161.224	161.930	163.215	161.612	0.1118	0.9639
DG	-	-	0.0804	0.0273	1.6110	0.4684	78.776	161.552	162.258	163.544	161.941	0.1039	0.9822
DEC	0.1186	0.1806	0.3237	0.0974	2.2727	2.4363	78.656	163.312	164.812	166.299	163.895	0.1102	0.9683
EDW	0.9914	0.0133	1.4962	0.3868	0.8545	0.3976	78.561	163.123	164.623	166.110	163.706	0.0840	0.9989
DMW	0.3585	0.4238	1.0158	0.0566	0.9885	0.0164	78.734	163.469	164.969	166.456	164.052	0.1430	0.8082
Data-2													
DPham	-	-	0.9297	0.1763	1.0052	0.0052	109.35	222.709	223.509	224.490	222.954	0.1078	0.9700
Geom	-	-	-	-	0.0058	0.0013	110.72	223.437	223.687	224.533	223.560	0.1264	0.9022
NB	-	-	1.1306	0.3418	172.15	38.294	110.64	225.275	226.075	227.056	225.521	0.1208	0.9273
DNH	-	-	1.5692	0.5207	0.0031	0.0013	110.13	224.255	225.055	226.035	224.500	0.1178	0.9391
DP	-	-	0.0085	0.0029	0.6999	0.9410	110.20	224.396	225.196	226.177	224.641	0.1091	0.9668
DW	-	-	1.0573	0.2190	149.37	33.091	110.84	225.688	226.488	227.469	225.934	0.1807	0.5400
DG	-	-	0.0066	0.0023	1.1390	0.3290	110.64	225.270	226.070	227.051	225.516	0.1215	0.9245
DEC	0.0072	0.0093	0.2975	0.0347	0.8835	0.4233	109.70	225.393	227.107	228.064	225.761	0.1102	0.9621
EDW	0.9956	0.0031	1.0615	0.1197	1.0675	0.3420	110.57	227.136	228.850	229.807	227.504	0.1230	0.9178
DMW	0.8202	0.0544	0.9199	0.0960	0.9978	0.0007	110.89	227.779	229.493	230.450	228.147	0.1134	0.9543
Data-3													
DPham	-	-	2.2002	0.1697	1.0026	0.0011	56.217	116.433	117.139	118.425	116.822	0.1567	0.7097
Geom	-	-	-	-	0.0858	0.0183	68.222	138.444	138.666	139.440	138.639	0.3665	0.0093
NB	-	-	12.849	9.8657	10.651	0.9870	58.113	120.226	120.932	122.217	120.615	0.1922	0.4507
DNH	-	-	18.008	12.512	0.0037	0.0026	63.249	130.498	131.204	132.489	130.886	0.3065	0.0467
DP	-	-	0.4006	0.0763	0.0110	0.0106	57.127	118.255	118.961	120.246	118.644	0.1636	0.6584
DW	-	-	2.9995	0.5589	12.473	0.9743	57.013	118.026	118.732	120.017	118.415	0.1223	0.9257
DG	-	-	0.4692	0.1530	5.2320	1.6288	58.824	121.649	122.355	123.640	122.038	0.1237	0.9195
DEC	0.0059	0.0052	0.6406	0.0489	1.0002	0.3792	56.329	118.659	120.159	121.646	119.242	0.1547	0.7245
EDW	0.9944	0.0042	2.1818	0.2647	1.4646	0.4894	57.622	121.245	122.745	124.232	121.828	0.1917	0.4541
DMW	0.9932	0.0064	1.8528	2.2912	1.2638	0.0620	56.541	119.082	120.582	122.069	119.665	0.1745	0.5766

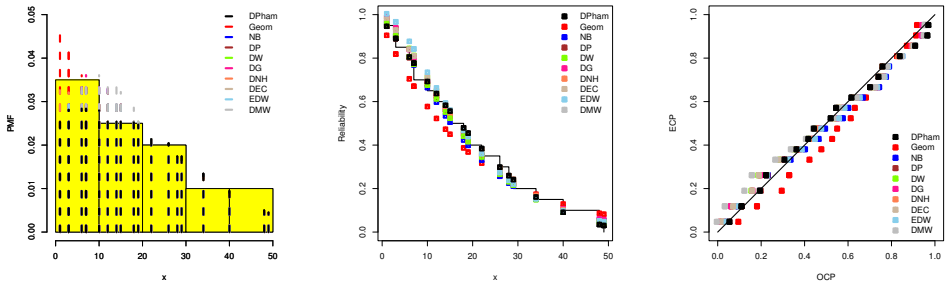

(a)-(i) PMF: Data-1 (a)-(ii) RF: Data-1 (a)-(iii) PP: Data-1

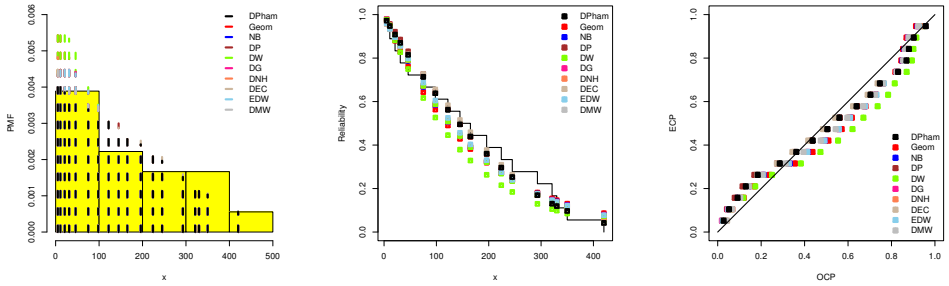

(b)-(i) PMF: Data-2 (b)-(ii) RF: Data-2 (b)-(iii) PP: Data-2

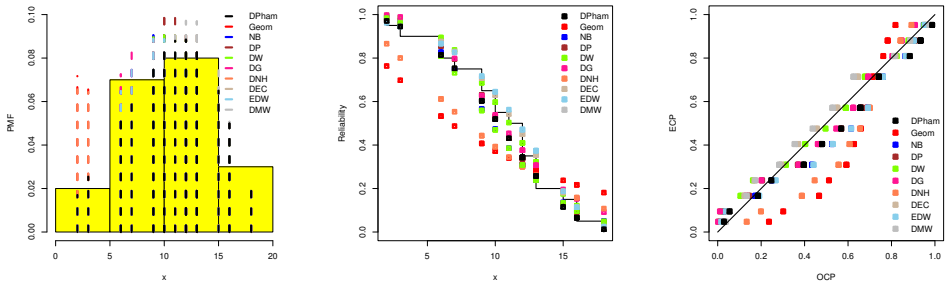

(c)-(i) PMF: Data-3 (c)-(ii) RF: Data-3 (c)-(iii) PP: Data-3

Figure 12. Visualization diagrams of the DPham and its competitors from three real datasets.

Table 10. Estimates of α (1^{st} row) and μ (2^{nd} row) from three real datasets.

Data	(n, r)	MLE / Bayes		ACI[NA] / ACI[NL]			BCI / HPD		
		Est.	SE	Low.	Upp.	Width	Low.	Upp.	Width
Data-1	(20,8)	1.3117	0.4597	0.4107	2.2128	1.8022	1.2193	1.3989	0.1796
		1.3097	0.0458	0.6600	2.6072	1.9473	1.2184	1.3976	0.1792
		1.0159	0.0188	0.9791	1.0528	0.0737	0.9145	1.1116	0.1971
		1.0130	0.0503	0.9797	1.0535	0.0738	0.9136	1.1105	0.1969
	(20,12)	1.2094	0.3393	0.5444	1.8745	1.3301	1.1239	1.2864	0.1625
		1.2067	0.0413	0.6979	2.0960	1.3981	1.1280	1.2901	0.1621
		1.0184	0.0187	0.9817	1.0552	0.0735	0.9175	1.1126	0.1951
		1.0162	0.0499	0.9823	1.0559	0.0735	0.9203	1.1144	0.1941
	(20,20)	1.0359	0.1992	0.6454	1.4264	0.7810	0.9685	1.0877	0.1191
		1.0317	0.0305	0.7106	1.5102	0.7996	0.9736	1.0922	0.1187
		1.0264	0.0198	0.9876	1.0653	0.0777	0.9263	1.1218	0.1954
		1.0242	0.0499	0.9883	1.0660	0.0777	0.9258	1.1204	0.1946
Data-2	(18,8)	0.8009	0.2810	0.2502	1.3517	1.1015	0.7208	0.8680	0.1473
		0.7966	0.0380	0.4027	1.5931	1.1904	0.7222	0.8692	0.1470
		1.0099	0.0136	0.9832	1.0366	0.0534	0.9086	1.1052	0.1966
		1.0071	0.0502	0.9835	1.0370	0.0534	0.9062	1.1021	0.1959
	(18,12)	0.8015	0.2244	0.3617	1.2414	0.8798	0.7335	0.8548	0.1213
		0.7970	0.0313	0.4630	1.3876	0.9246	0.7350	0.8560	0.1210
		1.0096	0.0117	0.9867	1.0326	0.0459	0.9100	1.1042	0.1942
		1.0069	0.0499	0.9869	1.0329	0.0459	0.9082	1.1019	0.1937
	(18,18)	0.9348	0.1995	0.5438	1.3259	0.7821	0.8840	0.9726	0.0885
		0.9308	0.0231	0.6152	1.4204	0.8051	0.8862	0.9739	0.0877
		1.0050	0.0058	0.9936	1.0165	0.0228	0.9081	1.1024	0.1943
		1.0030	0.0499	0.9937	1.0165	0.0228	0.9068	1.1008	0.1940
Data-3	(20,6)	2.0198	0.8225	0.4077	3.6320	3.2243	1.9242	2.1121	0.1879
		2.0183	0.0479	0.9092	4.4869	3.5777	1.9242	2.1121	0.1879
		1.0036	0.0066	0.9906	1.0166	0.0259	0.9030	1.0991	0.1961
		1.0010	0.0502	0.9907	1.0166	0.0259	0.9039	1.0997	0.1958
	(20,12)	2.3894	0.7032	1.0111	3.7676	2.7565	2.3007	2.4705	0.1698
		2.3868	0.0435	1.3420	4.2540	2.9119	2.3029	2.4722	0.1693
		1.0016	0.0029	0.9960	1.0073	0.0113	0.9016	1.0972	0.1956
		0.9993	0.0501	0.9960	1.0073	0.0113	0.9001	1.0947	0.1947
	(20,20)	2.2841	0.4550	1.3923	3.1759	1.7837	2.2093	2.3478	0.1385
		2.2810	0.0353	1.5458	3.3751	1.8293	2.2123	2.3502	0.1379
		1.0020	0.0026	0.9970	1.0071	0.0101	0.8998	1.0976	0.1978
		0.9990	0.0503	0.9970	1.0071	0.0101	0.8976	1.0946	0.1971

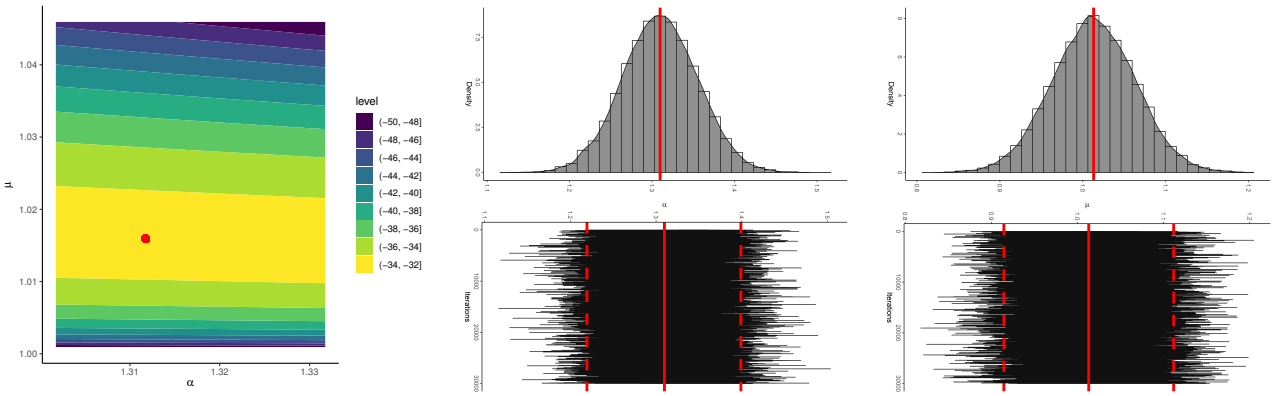

(a) Data-1 $(n, r) = (20, 8)$

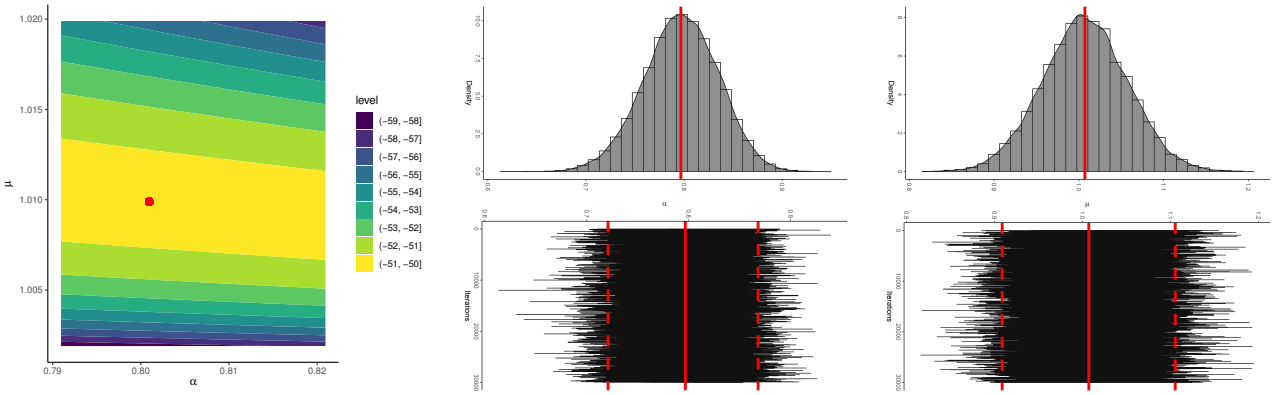

(b) Data-2 $(n, r) = (18, 8)$

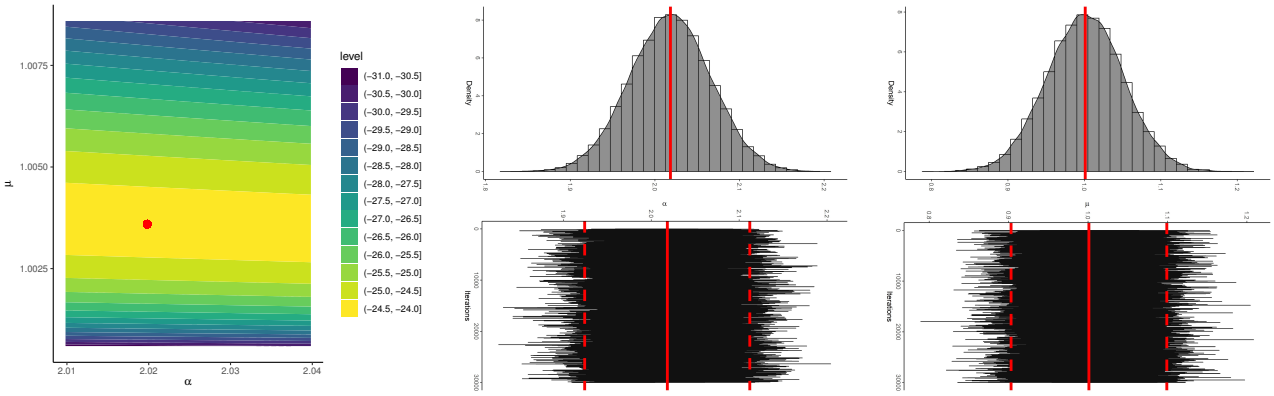

(c) Data-3 $(n, r) = (20, 6)$

Figure 13. The contour and trace/density diagrams of α and μ from three real datasets.

Table 11. Statistics of α (1^{st} row) and μ (2^{nd} row) from three real datasets.

Data	(n, r)	Mean	Mode	Q_1	Q_2	Q_3	SD	Skew.
Data-1	(20,8)	1.3097	1.2504	1.2787	1.3095	1.3406	0.0458	0.0050
		1.0130	0.9054	0.9793	1.0129	1.0467	0.0502	-0.0023
	(20,12)	1.2067	1.2014	1.1793	1.2074	1.2348	0.0412	-0.0741
		1.0162	0.9456	0.9826	1.0165	1.0501	0.0499	-0.0327
	(20,20)	1.0317	1.0253	1.0122	1.0325	1.0526	0.0302	-0.2105
		1.0242	0.9853	0.9905	1.0244	1.0585	0.0498	0.0044
Data-2	(18,8)	0.7966	0.8141	0.7717	0.7972	0.8227	0.0377	-0.1201
		1.0071	0.9424	0.9736	1.0066	1.0402	0.0501	0.0102
	(18,12)	0.7970	0.8056	0.7767	0.7984	0.8185	0.0310	-0.2201
		1.0069	0.9694	0.9732	1.0073	1.0403	0.0499	-0.0098
	(18,18)	0.9308	0.9192	0.9159	0.9320	0.9467	0.0227	-0.2575
		1.0030	0.9648	0.9695	1.0023	1.0363	0.0499	0.0564
Data-3	(20,6)	2.0183	2.0086	1.9858	2.0185	2.0506	0.0479	-0.0147
		1.0010	0.9048	0.9670	1.0012	1.0350	0.0502	-0.0069
	(20,12)	2.3868	2.3889	2.3581	2.3870	2.4163	0.0434	-0.0461
		0.9993	0.9071	0.9654	0.9991	1.0332	0.0501	0.0157
	(20,20)	2.2810	2.2813	2.2579	2.2818	2.3052	0.0352	-0.1437
		0.9990	0.9774	0.9651	0.9992	1.0330	0.0503	-0.0269

8. Concluding remarks

This study introduced a new discrete analogue of the Pham distribution, referred to as the DPham model, with the primary aim of extending the flexibility and interpretability of the continuous Pham framework to integer-valued lifetime and count data. By employing a survival-function-based discretization, the proposed model successfully preserves key structural features of the continuous Pham distribution while remaining analytically tractable and practically applicable to discrete settings commonly encountered in reliability engineering, actuarial science, biomedical studies, and risk analysis. The DPham distribution exhibits remarkable flexibility. Its probability mass function can assume decreasing, increasing, or unimodal forms, and its hazard rate function is capable of modeling increasing, constant, and V-tub (bathtub-shaped) aging behaviors. These properties allow the model to capture complex failure mechanisms, including early-life failures, random shocks during useful life, and wear-out phenomena. The derivation of core distributional properties, such as the quantile function, moments, dispersion measures, skewness, kurtosis, and order statistics, provides a comprehensive understanding of the model's behavior and highlights its ability to accommodate over-dispersion, heavy tails, and strong asymmetry, which are often observed in real-world discrete data. On the inferential side, the paper developed both classical and Bayesian estimation procedures under Type-II censoring schemes. The existence and uniqueness of the maximum likelihood estimators ensure inferential stability, and the Bayesian framework, implemented via MCMC methods, offers a flexible alternative when likelihood-based inference becomes challenging. The comparative investigation of

asymptotic confidence intervals, Bayesian credible intervals, and HPD intervals demonstrates that Bayesian intervals, particularly HPD intervals, tend to provide superior coverage accuracy and shorter interval lengths, especially in small samples and censored data scenarios. The extensive simulation study confirms the consistency, robustness, and efficiency of the proposed estimators, and the real-data applications illustrate the clear practical advantages of the DPham model over several well-established competing discrete distributions.

Based on the findings of this study, several recommendations can be made for practitioners. First, the DPham distribution is strongly recommended for modeling discrete lifetime or count data exhibiting nonmonotone hazard structures, overdispersion, or heavy-tailed behavior, where classical discrete models may fail. Second, in the presence of censoring or limited sample sizes, Bayesian inference using informative gamma priors and HPD intervals is advised, as it consistently yields more reliable point and interval estimates. Third, the availability of a closed-form quantile function makes the DPham model particularly suitable for simulation-based studies and Monte Carlo reliability assessments. The proposed DPham model also opens multiple avenues for future research. One natural extension is the development of regression and covariate-dependent versions of the DPham distribution, allowing model parameters to vary as functions of explanatory variables for use in discrete survival regression and generalized linear modeling frameworks. Another promising direction involves the construction of multivariate or bivariate DPham models to accommodate dependent discrete lifetimes or correlated count processes. Extensions to alternative censoring schemes, such as progressive, hybrid, or interval censoring, would further enhance the applicability of the model in practical life-testing experiments.

In summary, future work may explore alternative prior structures, hierarchical Bayesian formulations, or empirical Bayes approaches to improve inference further. Goodness-of-fit diagnostics, residual analysis, and information-theoretic model selection tools tailored specifically to the DPham framework would also be valuable additions. While the proposed DPham distribution effectively models over-dispersion and heavy-tailed count data, it does not explicitly account for zero-inflated scenarios. However, in practical applications with abundant zeros, zero-inflated models such as the zero-inflated Poisson or zero-inflated negative binomial may provide improved fit. Developing a zero-inflated extension of the DPham distribution constitutes an important direction for future research. Finally, applications of the DPham distribution to emerging fields, such as cyber-risk modeling, discrete degradation processes, epidemiological count data, and reliability analysis of modern engineered systems, represent fertile ground for further investigation. Overall, the DPham distribution provides a flexible, robust, and theoretically sound framework for modeling discrete lifetime and count data. Its strong inferential performance, combined with its ability to capture complex hazard and dispersion structures, makes it a valuable addition to the growing literature on discrete distribution theory and a practical tool for applied statisticians and reliability analysts.

Author contributions

Ahmed Elshahhat: Methodology, Writing–original draft, Writing–review & editing, Software; Osama E. Abo-Kasem: Methodology, Writing–review & editing; Heba S. Mohammed: Methodology, Funding acquisition, Writing–original draft, Writing–review & editing. All authors of this article have been contributed equally.

Use of Generative-AI tools declaration

The authors declare they have not used Artificial Intelligence (AI) tools in the creation of this article.

Funding

This research was funded by Princess Nourah bint Abdulrahman University Researchers Supporting Project number (PNURSP2026R175), Princess Nourah bint Abdulrahman University, Riyadh, Saudi Arabia.

Conflict of interest

There is no conflict of interest.

References

1. H. Pham, A vtub-shaped hazard rate function with applications to system safety, *Int. J. Reliab. Appl.*, **3** (2002), 1–16.
2. A. Srivastava, V. Kumar, Analysis of Pham (loglog) reliability model using Bayesian approach, *Computer Science Journal*, **1** (2011), 79–100.
3. S. Yang, D. Meng, H. Wang, C. Yang, A novel learning function for adaptive surrogate-model-based reliability evaluation, *Philos. Trans. A Math. Phys. Eng. Sci.*, **382** (2024), 20220395. https://doi.org/10.1098/rsta.2022.0395
4. M. La Rocca, M. Menzietti, C. Perna, M. Sibillo, *New perspectives in mathematical and statistical methods for actuarial sciences and finance*, Cham: Springer, 2026. https://doi.org/10.1007/978-3-032-05551-4
5. S. Singh, T. Madke, P. Chand, Global epidemiology of hepatocellular carcinoma, *J. Clin. Exp. Hepatol.*, **15** (2025), 102446. https://doi.org/10.1016/j.jceh.2024.102446
6. S. Yang, D. Meng, H. Yang, C. Luo, X. Su, Enhanced soft Monte Carlo simulation coupled with support vector regression for structural reliability analysis, *Proc. Ins. Civil Eng.-Transp.*, **178** (2025), 459–474. https://doi.org/10.1680/jtran.24.00128
7. D. Keefer, S. Bodily, Three-point approximations for continuous random variables, *Manage. Sci.*, **29** (1983), 595–609. https://doi.org/10.1287/mnsc.29.5.595
8. C. Lai, Issues concerning constructions of discrete lifetime models, *Qual. Technol. Quant. M.*, **10** (2013), 251–262. https://doi.org/10.1080/16843703.2013.11673320
9. K. Jayakumar, K. Sankaran, A generalization of discrete Weibull distribution, *Commun. Stat.-Theor. M.*, **47** (2018), 6064–6078. https://doi.org/10.1080/03610926.2017.1406115
10. A. Afify, M. Ahsan-ul-Haq, H. Aljohani, A. Alghamdi, A. Babar, H. Gómez, A new one-parameter discrete exponential distribution: properties, inference, and applications to COVID-19 data, *J. King Saud Univ. Sci.*, **34** (2022), 102199. https://doi.org/10.1016/j.jksus.2022.102199

11. C. Augusto Taconeli, I. Rodrigues de Lara, Discrete Weibull distribution: different estimation methods under ranked set sampling and simple random sampling, *J. Stat. Comput. Sim.*, **92** (2022), 1740–1762. https://doi.org/10.1080/00949655.2021.2005597
12. D. Roy, R. Gupta, Characterizations and model selections through reliability measures in the discrete case, *Stat. Probabil. Lett.*, **43** (1999), 197–206. https://doi.org/10.1016/S0167-7152(98)00260-0
13. D. Roy, T. Ghosh, A new discretization approach with application in reliability estimation, *IEEE Trans. Reliab.*, **58** (2009), 456–461. https://doi.org/10.1109/TR.2009.2028093
14. M. Bebbington, C. Lai, M. Wellington, R. Zitikis, The discrete additive Weibull distribution: a bathtub-shaped hazard for discontinuous failure data, *Reliab. Eng. Syst. Safe.*, **106** (2012), 37–44. https://doi.org/10.1016/j.ress.2012.06.009
15. H. Haj Ahmad, A. Elshahhat, A new hjorth distribution in its discrete version, *Mathematics*, **13** (2025), 875. https://doi.org/10.3390/math13050875
16. A. Eldeeb, M. Ahsan-ul-Haq, A. Babar, A new discrete XLindley distribution: theory, actuarial measures, inference, and applications, *Int. J. Data Sci. Anal.*, **17** (2024), 323–333. https://doi.org/10.1007/s41060-023-00395-8
17. A. Elshahhat, H. Rezk, R. Alotaibi, The discrete Gompertz-Makeham distribution for multidisciplinary data analysis, *AIMS Mathematics*, **10** (2025), 17117–17178. https://doi.org/10.3934/math.2025768
18. A. Elshahhat, H. Rezk, R. Alotaibi, A new one-parameter model by extending Maxwell-Boltzmann theory to discrete lifetime modeling, *Mathematics*, **13** (2025), 2803. https://doi.org/10.3390/math13172803
19. A. Fayomi, A. Ahmed, N. AL-Sayed, S. Behairy, A. Abd AL-Fattah, G. AL-Dayian, et al., Constant stress-partially accelerated life tests of V-tub shaped lifetime distribution under progressive type II censoring, *Symmetry*, **16** (2024), 1251. https://doi.org/10.3390/sym16091251
20. O. Alqasem, M. Nassar, M. Elmahi Abd Elwahab, A. Elshahhat, A new inverted Pham distribution for data modeling of mechanical components and diamond in South-West Africa, *Phys. Scr.*, **99** (2024), 115268. https://doi.org/10.1088/1402-4896/ad8706
21. L. Djeumeni, S. Nadarajah, B. Engoulou, L. Fono, E. Wansouwe, On the (Hoang) Pham distribution, *Int. J. Reliab. Qual. Sa.*, **33** (2026), 2550048. https://doi.org/10.1142/S0218539325500482
22. A. Henningsen, O. Toomet, *maxLik*: a package for maximum likelihood estimation in R, *Comput. Stat.*, **26** (2011), 443–458. https://doi.org/10.1007/s00180-010-0217-1
23. M. Plummer, N. Best, K. Cowles, K. Vines, CODA: convergence diagnosis and output analysis for MCMC, *R News*, **6** (2006), 7–11.
24. J. Lawless, *Statistical models and methods for lifetime data*, Hoboken: John Wiley and Sons, 2003. https://doi.org/10.1002/9781118033005
25. W. Meeker, L. Escobar, F. Pascual, *Statistical methods for reliability data*, New York: John Wiley and Sons, 2014.

26. D. Kundu, Bayesian inference and life testing plan for the Weibull distribution in presence of progressive censoring, *Technometrics*, **50** (2008), 144–154. https://doi.org/10.1198/004017008000000217

27. H. Bakouch, M. Jazi, S. Nadarajah, A new discrete distribution, *Statistics*, **48** (2014), 200–240. https://doi.org/10.1080/02331888.2012.716677

28. M. Eliwa, M. El-Morshedy, A one-parameter discrete distribution for over-dispersed data: Statistical and reliability properties with applications, *J. Appl. Stat.*, **49** (2022), 2467–2487. https://doi.org/10.1080/02664763.2021.1905787

29. F. Wang, A new model with bathtub-shaped failure rate using an additive Burr XII distribution, *Reliab. Eng. Syst. Safe.*, **70** (2000), 305–312. https://doi.org/10.1016/S0951-8320(00)00066-1

30. A. Elshahhat, W. Abu El Azm, Statistical reliability analysis of electronic devices using generalized progressively hybrid censoring plan, *Qual. Reliab. Eng. Int.*, **38** (2022), 1112–1130. https://doi.org/10.1002/qre.3058

31. D. Murthy, M. Xie, R. Jiang, *Weibull models*, Hoboken: John Wiley, 2004. https://doi.org/10.1002/047147326X

32. G. Cordeiro, M. Lima, A. Cysneiros, M. Pascoa, R. Pescim, E. Ortega, An extended Birnbaum-Saunders distribution: theory, estimation, and applications, *Commun. Stat.-Theor. M.*, **45** (2016), 2268–2297. https://doi.org/10.1080/03610926.2013.879182

33. N. Johnson, A. Kemp, S. Kotz, *Univariate discrete distributions*, New York: John Wiley and Sons, 2005. https://doi.org/10.1002/0471715816

34. M. Shafqat, S. Ali, I. Shah, S. Dey, Univariate discrete Nadarajah and Haghighi distribution: properties and different methods of estimation, *Statistica*, **80** (2020), 301–330. https://doi.org/10.6092/issn.1973-2201/9532

35. A. Tyagi, N. Choudhary, B. Singh, A new discrete distribution: theory and applications to discrete failure lifetime and count data, *J. Appl. Probab. Stat.*, **15** (2020), 117–143.

36. T. Nakagawa, S. Osaki, The discrete Weibull distribution, *IEEE Trans. Reliab.*, **R-24** (1975), 300–301. https://doi.org/10.1109/TR.1975.5214915

37. S. Chakraborty, D. Chakravarty, Discrete gamma distributions: properties and parameter estimations, *Commun. Stat.-Theor. M.*, **41** (2012), 3301–3324. https://doi.org/10.1080/03610926.2011.563014

38. R. Alotaibi, H. Rezk, C. Park, A. Elshahhat, The discrete exponentiated-Chen model and its applications, *Symmetry*, **15** (2023), 1278. https://doi.org/10.3390/sym15061278

39. V. Nekoukhou, H. Bidram, The exponentiated discrete Weibull distribution, *Sort-Stat. Oper. Res. Trans.*, **39** (2015), 127–146.

40. S. Almalki, S. Nadarajah, A new discrete modified Weibull distribution, *IEEE Trans. Reliab.*, **63** (2014), 68–80. https://doi.org/10.1109/TR.2014.2299691

Appendix 1. The probability mass function

Consider $X \sim \text{DPham}(\alpha, \mu)$ with parameters $\alpha > 0$ and $\mu > 1$; following the discretizing SF-based method, the PMF of X becomes

$$\mathsf{P}(x;\boldsymbol{\theta}) = \mathsf{S}(x) - \mathsf{S}(x+1) = \exp(1-\mu^{x^{\alpha}}) - \exp(1-\mu^{(x+1)^{\alpha}}), \tag{A1.1}$$

which satisfies the following properties (for $\Delta = \mathsf{S}(x-1) - 2\mathsf{S}(x) + \mathsf{S}(x+1)$):

(i) $\mathsf{P}(x)$ is decreasing when $\Delta \geq 0$ for all x;
(ii) $\mathsf{P}(x)$ is increasing when $\Delta \leq 0$ for all x;
(iii) $\mathsf{P}(x)$ is unimodal when the sign changes once.

Proof. The shape of $\mathsf{P}(x)$ depends on the behavior of the discrete second difference of $\mathsf{S}(x)$:

$$\Delta = \mathsf{P}(x+1) - \mathsf{P}(x) = [\mathsf{S}(x) - \mathsf{S}(x+1)] - [\mathsf{S}(x-1) - \mathsf{S}(x)] = \mathsf{S}(x-1) - 2\mathsf{S}(x) + \mathsf{S}(x+1).$$

Thus, the monotonicity of $\mathsf{P}(x)$ is governed by the discrete convexity or concavity of $\mathsf{S}(x)$:

- If $\Delta \geq 0$ for all x, then $\mathsf{P}(x)$ is decreasing.
- If $\Delta \leq 0$ for all x, then $\mathsf{P}(x)$ is increasing.
- If the sign changes once, $\mathsf{P}(x)$ is unimodal.

To analyze this, extend $\mathsf{S}(x)$ to the continuous domain $x > -1$:

$$\mathsf{S}(x) = \exp(1 - \mathsf{h}(x)), \quad \text{where } \mathsf{h}(x) := \mu^{(x+1)^{\alpha}}.$$

The convexity of S relates to the curvature of h. Computing derivatives, we have

$$\mathsf{h}^{\star}(x) = \mu^{(x+1)^{\alpha}} \log(\mu) \cdot \alpha(x+1)^{\alpha-1},$$

and

$$\mathsf{h}^{\star\star}(x) = \mu^{(x+1)^{\alpha}} \log(\mu) \cdot \alpha(x+1)^{\alpha-2} \left[(\alpha-1) + \alpha(x+1)^{\alpha} \log(\mu)\right].$$

Because $\mu > 1$, $\mu^{(x+1)^{\alpha}} > 0$, and $\log(\mu) > 0$, the sign of $\mathsf{h}^{\star\star}(x)$ depends on the bracketed term

$$\wp(x) := (\alpha - 1) + \alpha(x+1)^{\alpha} \log(\mu).$$

Case 1. $0 < \alpha \leq 1$**:** Here, $\alpha - 1 \leq 0$ For all $x \geq 0$, the positive term $\alpha(x+1)^{\alpha} \log(\mu)$ may not be large enough to compensate for the negative $\alpha - 1$ when μ is moderate. Thus, $\wp(x)$ can remain negative or close to zero, implying $\mathsf{h}^{\star\star}(x) \leq 0$ or near zero in many practical cases. Hence, $\mathsf{h}(x)$ is concave or nearly linear, and $\mathsf{S}(x) = \exp(1 - \mathsf{h}(x))$ is convex or approximately convex, making the PMF $\mathsf{P}(x)$ *monotonically decreasing*.

Case 2. $\alpha > 1$**:** Now, $\alpha - 1 > 0$. Thus,

$$\wp(x) = (\alpha - 1) + \alpha(x+1)^{\alpha} \log(\mu) > 0,$$

for all x because all terms are positive. Consequently, $\mathsf{h}^{\star\star}(x) > 0$ for all x, so h is strictly convex and increasing rapidly. This implies $\mathsf{S}(x)$ is concave near the origin, and $\mathsf{P}(x)$ is initially *increasing* in x for small values.

Case 3. Large α and $\mu \approx 1$: For large α, the term $\alpha(x+1)^{\alpha}\log(\mu)$ dominates for moderate to large x. Initially, due to the large positive $\alpha - 1$, $\mathsf{h}^{\star\star}(x)$ is positive and $\mathsf{P}(x)$ increases. However, as x grows further, the exponential terms cause $\mathsf{P}(x)$ to eventually decrease due to the dominant decay in the PMF tails. This yields a *unimodal* PMF with a single mode at some finite x^{*}.

Hence, depending on α, the PMF $\mathsf{P}(x)$ of the DPham distribution can be decreasing, increasing, or unimodal, confirming the observed shapes in the subplots shown in Figure 1. □

Appendix 2. The hazard function

Let X be a discrete random variable following the discrete Pham distribution, denoted by $X \sim \text{DPham}(\alpha, \mu)$, with parameters $\alpha > 0$ and $\mu > 1$. From the PMF (2.4) and CDF (2.5), the discrete HRF of X is given by

$$\mathsf{h}(x;\boldsymbol{\theta}) = \frac{\mathsf{P}(x;\boldsymbol{\theta})}{\mathsf{S}(x;\boldsymbol{\theta})} = 1 - \exp\Big(\mu^{x^{\alpha}} - \mu^{(x+1)^{\alpha}}\Big), \qquad x = 0, 1, 2, \ldots \tag{A2.1}$$

and satisfies the following properties:

(i) $\mathsf{h}(x)$ is increasing for $\alpha > 1$;
(ii) $\mathsf{h}(x)$ is constant for $\alpha = 1$;
(iii) $\mathsf{h}(x)$ is bathtub-shaped (V-tub) for $0 < \alpha < 1$.

Proof. Define

$$\nabla(x) = \mu^{x^{\alpha}} - \mu^{(x+1)^{\alpha}}, \qquad x \geq 0. \tag{A2.2}$$

Because the exponential function is strictly increasing, it follows that $1 - \exp(\nabla(x))$ is strictly *decreasing* in $\nabla(x)$. Hence, the monotonic behavior of $\mathsf{h}(x)$ is completely determined by that of $\nabla(x)$.

To analyze $\nabla(x)$, consider the continuous extension

$$\mathfrak{I}(x) = \mu^{x^{\alpha}}, \qquad x > 0, \tag{A2.3}$$

so that,

$$\nabla(x) = \mathfrak{I}(x) - \mathfrak{I}(x+1).$$

The first and second derivatives of $\mathfrak{I}(x)$ are

$$\mathfrak{I}'(x) = \mu^{x^{\alpha}} \log(\mu)\, \alpha x^{\alpha-1}, \tag{A2.4}$$

and

$$\mathfrak{I}''(x) = \mu^{x^{\alpha}} \log(\mu)\, \alpha x^{\alpha-2}\Big[(\alpha - 1) + \alpha x^{\alpha}\log(\mu)\Big]. \tag{A2.5}$$

Because $\mu > 1$, all multiplicative factors outside the bracket are strictly positive. Therefore, the sign of $\mathfrak{I}''(x)$ is governed by

$$(\alpha - 1) + \alpha x^{\alpha}\log(\mu).$$

Case 1. $\alpha > 1$: In this case, $\alpha - 1 > 0$, implying

$$(\alpha - 1) + \alpha x^{\alpha}\log(\mu) > 0 \quad \text{for all } x > 0.$$

Thus, $\mathfrak{I}(x)$ is strictly convex on $(0, \infty)$, and hence, $\mathfrak{I}(x+1) - \mathfrak{I}(x)$ is increasing in x. Consequently, $\nabla(x) = \mathfrak{I}(x) - \mathfrak{I}(x+1)$ is decreasing in x, which implies that $\mathsf{h}(x)$ is increasing.

Case 2. $\alpha = 1$: When $\alpha = 1$,

$$\nabla(x) = \mu^x - \mu^{x+1} = -\mu^x(\mu - 1),$$

which differs only by a multiplicative constant across x. Therefore, the hazard rate $\mathsf{h}(x)$ is constant.

Case 3. $0 < \alpha < 1$: Here, $\alpha - 1 < 0$. For sufficiently small x,

$$(\alpha - 1) + \alpha x^{\alpha} \log(\mu) < 0,$$

so $\mathfrak{I}(x)$ is concave, and $\nabla(x)$ is increasing. As $x \to \infty$,

$$\alpha x^{\alpha} \log(\mu) \to \infty,$$

and hence, $\mathfrak{I}(x)$ eventually becomes convex, implying that $\nabla(x)$ first increases and then decreases. Accordingly, $\mathsf{h}(x)$ is initially decreasing and then increasing, exhibiting a bathtub-shaped (V-tub) behavior. This completes the proof. □

Appendix 3. The quantile function

Starting from the CDF (2.5), we proceed algebraically to derive an explicit symbolic expression for the quantile function of the DPham($\boldsymbol{\theta}$) distribution, as outlined below:

$$\mathsf{Q}(u; \boldsymbol{\theta}) = \mathsf{F}^{-1}(\boldsymbol{\theta}; x+1) = \min\{x \in (0, 1, 2, \ldots) : F(x+1; \boldsymbol{\theta}) \geq u\};$$

hence,

$$\mathsf{Q}(u; \boldsymbol{\theta}) = \left\lceil \frac{\ln\left(1 - \ln\left(1-u\right)\right)}{\ln(\mu)} \right\rceil^{\frac{1}{\alpha}} - 1, \quad 0 < u < 1. \tag{A3.1}$$

Proof. The quantile function $Q(u)$ is defined as the solution of the equation $F(x) = u$, where $0 < u < 1$. Setting

$$u = 1 - \exp\left(1 - \mu^{(x+1)^{\alpha}}\right),$$

we obtain

$$\exp\left(1 - \mu^{(x+1)^{\alpha}}\right) = 1 - u.$$

Taking the natural logarithm on both sides yields

$$1 - \mu^{(x+1)^{\alpha}} = \ln(1-u).$$

Rearranging terms, we have

$$\mu^{(x+1)^{\alpha}} = 1 - \ln(1-u).$$

Applying the natural logarithm again gives

$$(x+1)^{\alpha} \ln(\mu) = \ln(1 - \ln(1-u)).$$

Because $0 < \mu < 1$, it follows that $\ln(\mu) < 0$, and hence,

$$(x+1)^{\alpha} = \frac{\ln(1 - \ln(1-u))}{\ln(\mu)}.$$

Taking the αth root of both sides leads to

$$x + 1 = \left[\frac{\ln(1 - \ln(1 - u))}{\ln(\mu)}\right]^{1/\alpha}.$$

Therefore, the quantile function is

$$Q(u) = \left[\frac{\ln(1 - \ln(1 - u))}{\ln(\mu)}\right]^{1/\alpha} - 1,$$

which completes the proof. □

Appendix 4. The existence and uniqueness of MLE

Let $\mathbf{x} = (x_1 \leq \cdots \leq x_r)$ denote the observed failure times from a sample of size n from the CT2 scheme. Consider the log-LF

$$\mathsf{L}^{\star}(\boldsymbol{\theta}|\mathbf{x}) \propto \sum_{i=1}^{r} \log\left[\exp\left(1 - \mu^{x_i^{\alpha}}\right) - \exp\left(1 - \mu^{(x_i+1)^{\alpha}}\right)\right] + (n - r)\left[1 - \mu^{(x_r+1)^{\alpha}}\right],$$

where $\mu > 1$ and $\alpha > 0$. Then, the MLEs of α and μ exist and are unique.

Proof. The proof is established by examining the behavior and monotonicity of the log-LF with respect to each parameter.

Step 1. Existence and uniqueness of the MLE of μ: Fix $\alpha > 0$, and regard $\mathsf{L}^{\star}(\boldsymbol{\theta}|\mathbf{x})$ as a function of $\mu > 1$. Because $\mu^{x^{\alpha}}$ is strictly increasing in μ, the function

$$\exp\left(1 - \mu^{x_i^{\alpha}}\right) - \exp\left(1 - \mu^{(x_i+1)^{\alpha}}\right)$$

is strictly positive and continuous for all $\mu > 1$. Moreover,

$$\lim_{\mu \to 1^+} \mathsf{L}^{\star}(\boldsymbol{\theta}|\mathbf{x}) = -\infty, \qquad \lim_{\mu \to \infty} \mathsf{L}^{\star}(\boldsymbol{\theta}|\mathbf{x}) = -\infty,$$

which guarantees the existence of at least one maximizer $\hat{\mu} > 1$ by continuity.

The score function (4.5) with respect to μ is

$$\frac{\partial \mathsf{L}^{\star}}{\partial \mu} = \sum_{i=1}^{r} \left[\frac{\zeta^{\bullet}(x_i + 1; \alpha, \mu) - \zeta^{\bullet}(x_i; \alpha, \mu)}{\zeta(x_i; \alpha, \mu)}\right] + (n - r)\,\zeta^{\bullet}(x_r + 1; \alpha, \mu). \tag{A4.1}$$

Each term in (A4.1) is a strictly decreasing function of μ on $(1, \infty)$ due to the exponential dominance of $\mu^{(x+1)^{\alpha}}$ over $\mu^{x^{\alpha}}$. Therefore, the score function (4.5) is strictly decreasing in μ, and the LF equation admits a unique solution.

Step 2. Existence and uniqueness of the MLE of α: Fix $\mu > 1$, and consider $\mathsf{L}^{\star}(\boldsymbol{\theta}|\mathbf{x})$ as a function of $\alpha > 0$. Because x^{α} is strictly increasing in α for $x > 1$, the log-LF is continuous on $(0, \infty)$. Furthermore,

$$\lim_{\alpha \to 0^+} \mathsf{L}^{\star}(\boldsymbol{\theta}|\mathbf{x}) = -\infty, \qquad \lim_{\alpha \to \infty} \mathsf{L}^{\star}(\boldsymbol{\theta}|\mathbf{x}) = -\infty,$$

ensuring the existence of at least one maximizer $\hat{\alpha} > 0$.

The score function (4.5) with respect to α is

$$\frac{\partial \mathsf{L}^{\star}}{\partial \alpha} = \sum_{i=1}^{r} \left[\frac{\zeta^{\circ}(x_i + 1; \alpha, \mu) - \zeta^{\circ}(x_i; \alpha, \mu)}{\zeta(x_i; \alpha, \mu)} \right] + (n - r)\, \zeta^{\circ}(x_r + 1; \alpha, \mu). \tag{A4.2}$$

Because $\mu > 1$, it follows that $\ln(\mu) > 0$. Moreover, the term $x \mapsto x^{\alpha} \ln(x) \mu^{x^{\alpha}}$ is strictly increasing in α for $x > 1$. Consequently, the expression inside the square brackets in (A4.2) is strictly increasing in α. Because it is multiplied by $-\ln(\mu) < 0$, the score function $\partial \mathsf{L}^{\star}/\partial \alpha$ is strictly decreasing in α. Hence, the LF equation $\partial \mathsf{L}^{\star}/\partial \alpha = 0$ admits a unique solution.

Step 3. Joint uniqueness: Because the log-LF admits a unique maximizer in each parameter conditionally and is continuous on $(\alpha, \mu) \in (0, \infty) \times (1, \infty)$, the joint MLE $(\hat{\alpha}, \hat{\mu})$ exists and is unique. This completes the proof. □